#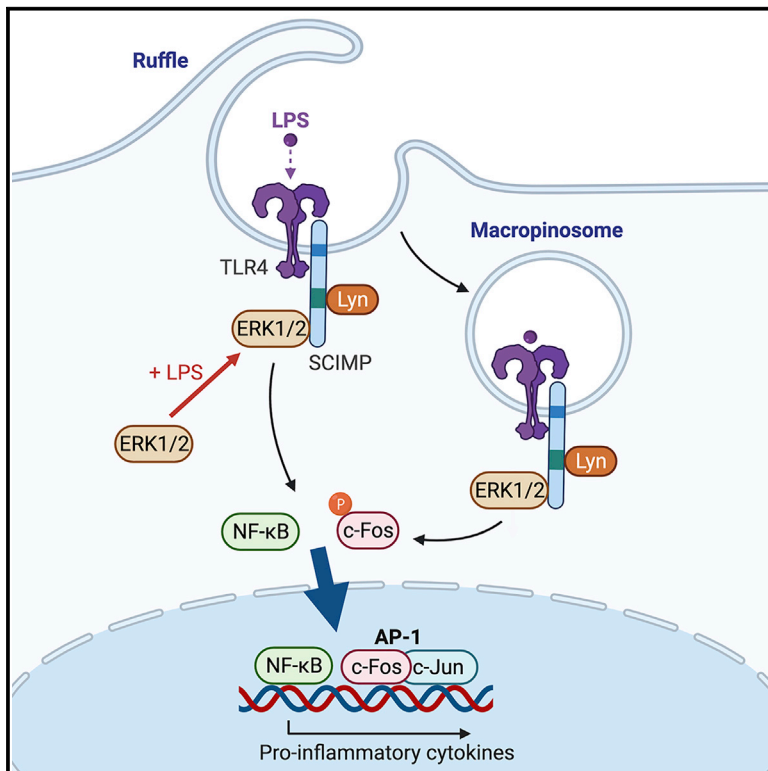 SCIMP is a spatiotemporal transmembrane scaffold for Erk1/2 to direct pro-inflammatory signaling in TLR-activated macrophages

Graphical abstract

Authors

Richard M. Lucas, Liping Liu, James E.B. Curson, ..., Matthew J. Sweet, Jennifer L. Stow, Lin Luo

Correspondence

l.luo@imb.uq.edu.au (L.L.), j.stow@imb.uq.edu.au (J.L.S.)

In brief

SCIMP is an immune-specific, transmembrane TLR adaptor genetically associated with inflammatory diseases. In this paper, Lucas et al. show that TLR-activated SCIMP scaffolds the signaling kinase Erk1/2, recruiting it to the cell surface to drive pro-inflammatory cytokine responses in macrophages. Targeting of SCIMP may dampen pro-inflammatory responses in disease settings.

Highlights

- Immune-specific TLR adaptor SCIMP is a scaffold for MAPK Erk1/2 in macrophages

- SCIMP recruits Erk2 to cell surface ruffles and macropinosomes for TLR signaling

- SCIMP-scaffolded Erk1/2 activates c-Fos to drive pro-inflammatory cytokine production

Article

SCIMP is a spatiotemporal transmembrane scaffold for Erk1/2 to direct pro-inflammatory signaling in TLR-activated macrophages

Richard M. Lucas,[1] Liping Liu,[1] James E.B. Curson,[1] Yvette W.H. Koh,[1] Neeraj Tuladhar,[1] Nicholas D. Condon,[1] Kaustav Das Gupta,[1] Sabrina S. Burgener,[1] Kate Schroder,[1] Evan Ingley,[2,3] Matthew J. Sweet,[1] Jennifer L. Stow,[1,*] and Lin Luo[1,4,*]

[1]Institute for Molecular Bioscience (IMB) and IMB Centre for Inflammation and Disease Research, The University of Queensland, Brisbane, QLD 4072, Australia
[2]Cell Signalling Group, Harry Perkins Institute of Medical Research and Centre for Medical Research, The University of Western Australia, Perth, WA 6009, Australia
[3]Discipline of Medical, Molecular and Forensic Sciences, College of Science, Health, Engineering and Education, Murdoch University, Murdoch, WA 6150, Australia
[4]Lead contact
*Correspondence: l.luo@imb.uq.edu.au (L.L.), j.stow@imb.uq.edu.au (J.L.S.)
https://doi.org/10.1016/j.celrep.2021.109662

SUMMARY

Immune cells are armed with Toll-like receptors (TLRs) for sensing and responding to pathogens and other danger cues. The role of extracellular-signal-regulated kinases 1/2 (Erk1/2) in TLR signaling remains enigmatic, with both pro- and anti-inflammatory functions described. We reveal here that the immune-specific transmembrane adaptor SCIMP is a direct scaffold for Erk1/2 in TLR pathways, with high-resolution, live-cell imaging revealing that SCIMP guides the spatial and temporal recruitment of Erk2 to membrane ruffles and macropinosomes for pro-inflammatory TLR4 signaling. SCIMP-deficient mice display defects in Erk1/2 recruitment to TLR4, c-Fos activation, and pro-inflammatory cytokine production, with these effects being phenocopied by Erk1/2 signaling inhibition. Our findings thus delineate a selective role for SCIMP as a key scaffold for the membrane recruitment of Erk1/2 kinase to initiate TLR-mediated pro-inflammatory responses in macrophages.

INTRODUCTION

Immune cells propagate signals from specific receptors through the recruitment of a diverse suite of cytoplasmic signaling molecules to specific membrane domains. Toll-like receptors (TLRs) are a well-studied family of immune receptors that detect pathogen or damage-associated signatures to elicit programs of pro- and anti-inflammatory cytokines and other innate immune responses (Akira and Takeda, 2004; Medzhitov, 2001). TLRs on the plasma membrane, endosomes, or macropinosomes are paired with specific sets of signaling adaptors (MyD88, Mal, TRIF, and TRAM), which trigger cascades of signaling kinases, including mitogen-activated protein kinases (MAPKs), to activate inflammatory transcription factors, such as nuclear factor κB (NF-κB), activator protein 1 (AP-1), CCAAT/enhancer binding protein β (C/EBPβ), and interferon regulatory factors (IRFs) (Kawai and Akira, 2007; Lu et al., 2009; Schmitz et al., 2007; Smolinska et al., 2011). These activated transcription factors then drive specific inflammatory cytokine production (Luo et al., 2019; O'Neill and Bowie, 2007).

The MAPK extracellular-signal-regulated kinase 1/2 (Erk1/2) plays a key role in TLR-mediated inflammatory pathways, stimulating both pro- and anti-inflammatory cytokine production as well as regulating expression of TLRs themselves in response to activation (An et al., 2002; Dumitru et al., 2000; Eliopoulos et al., 2003). In many other cell types and receptor-signaling pathways, Erk1/2 is recruited to activated receptors, such as receptor tyrosine kinases (RTKs) and G protein coupled receptors (GPCRs) by scaffold proteins, including IQ-motif containing Ras GTPase-activating-like proteins (IQGAPs), p21-activated kinase 1 (PAK1), caveolae-associated protein 4 (CAVIN4), paxillin, and β arrestins, which help to confine Erk1/2 activation and signaling to specific receptor-associated locales and pathways within cells (Casar and Crespo, 2016; Lavoie et al., 2020; Ogata et al., 2014). Activation of Erk1/2 during TLR-mediated inflammatory responses involves kinase signaling cascades, including the TPL2/MEK/Erk module (Banerjee et al., 2006; Kuriakose et al., 2014). However, these upstream elements do not provide a mechanism for spatiotemporal recruitment of Erk1/2 to activated TLRs in order to direct distinct pro- or anti-inflammatory immune signaling.

SLP adaptor and C-terminal Src kinase (CSK)-interacting membrane protein (SCIMP) is an immune-specific, transmembrane-signaling adaptor and a member of the palmitoylated transmembrane adaptor protein (pTRAP) family (Curson et al., 2018; Stepanek et al., 2014). It drives Erk1/2 signaling downstream of major histocompatibility complex type II (MHC II) and dectin-1 receptors in B cells and dendritic cells (DCs) (Draber
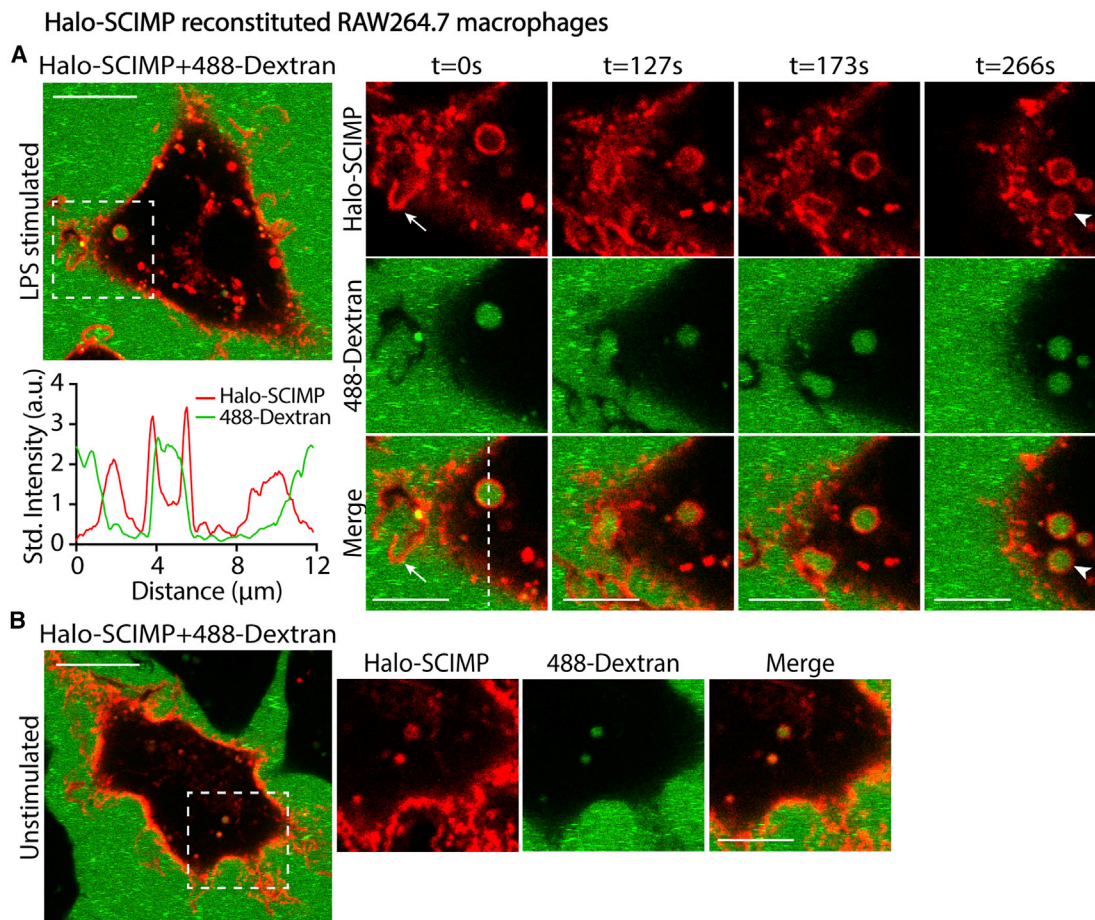
Halo-SCIMP reconstituted RAW264.7 macrophages

Figure 1. SCIMP is internalized on macropinosomes in response to LPS
Live imaging of CRISPR-Cas9-mediated SCIMP knockout RAW264.7 cells expressing Halo-SCIMP (red) incubated with 488-Dextran-70k (green) prior to imaging. Time series of cells stimulated with 100 ng/mL LPS for 30 min (A) shows SCIMP localized to cell surface ruffles (arrows) and internalized dextran-positive macropinosomes (arrowheads). Standardized intensity profiles of Halo-SCIMP and 488-Dextran across the macropinosome (dashed line) quantified for individual channels are shown. Unstimulated cells are shown in (B). All images are from a single experiment. Scale bar: 10 μm (inset scale bar: 5 μm).

et al., 2011; Kralova et al., 2016). In macrophages, SCIMP is a TLR-interacting protein that promotes receptor phosphorylation and transient MAPK signaling responses, including Erk1/2 (Luo et al., 2017). Phosphorylated SCIMP functions as a signaling adaptor and membrane scaffold for an array of effectors, including Src kinases. SCIMP paired with TLR4 or other cell-surface and intracellular TLRs acts to initiate a notably selective program of pro-inflammatory cytokines (Luo et al., 2017, 2020), and most recently, SCIMP has been implicated in inflammasome-driven interleukin-1β (IL-1β) production (Zewinger et al., 2020). Indeed, SCIMP is increasingly associated with autoimmune and pro-inflammatory-driven diseases (Dozmorov et al., 2014; Jansen et al., 2019).

In this study, we employ binding partner screens and high-resolution, live-cell imaging to reveal that Erk1/2 is recruited by SCIMP to dynamic membrane domains in response to TLR4 stimulation. Using signaling and cytokine assays, we describe a key signaling and transcriptional mechanism downstream of TLR4 and SCIMP for Erk1/2-mediated c-Fos and NF-κB activation and pro-inflammatory cytokine expression. Our results

reveal SCIMP as an important transmembrane TLR adaptor for scaffolding Erk1/2 at specific membrane signaling domains in macrophages, providing a mechanism for spatiotemporally recruiting Erk1/2 to TLRs for pro-inflammatory responses.

RESULTS

SCIMP is positioned at TLR4 signaling sites on ruffles and macropinosomes

As a transmembrane TLR adaptor and pTRAP, SCIMP is clustered in tetraspanin-enriched microdomains (TEMs) and detergent-resistant lipid membrane domains along with receptors, integrins, and tetraspanins (Horejsí et al., 2004; Curson et al., 2018). We and others have shown that TLR signaling adaptors and kinases are clustered on cell-surface ruffles and the macropinosomes arising from them in activated macrophages (Kagan et al., 2008; Luo et al., 2014a). Staining of SCIMP on fixed cells revealed that it localizes to cell surface protrusions, including filopodia and dorsal ruffles (Figure S1A; Luo et al., 2017). To examine SCIMP behavior in live cells, we performed live-cell imaging using
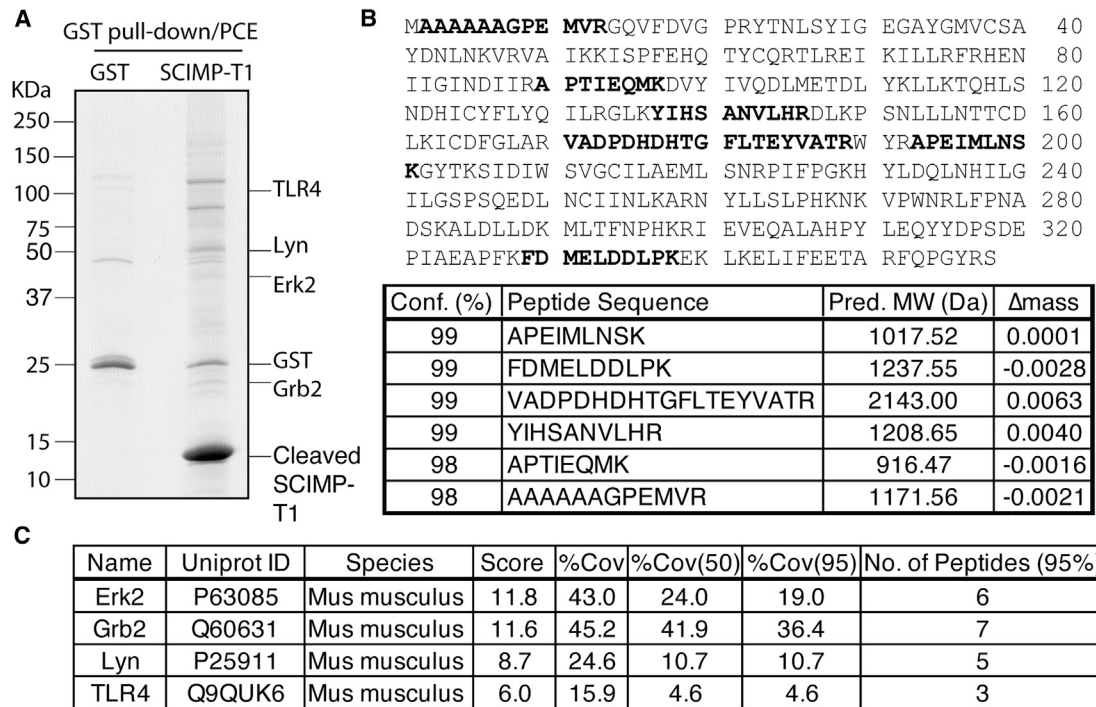
A

GST pull-down/PCE

B

```
MAAAAAAGPE MVRGQVFDVG PRYTNLSYIG EGAYGMVCSA   40
YDNLNKVRVA IKKISPFEHQ TYCQRTLREI KILLRFRHEN   80
IIGINDIIRA PTIEQMKDVY IVQDLMETDL YKLLKTQHLS  120
NDHICYFLYQ ILRGLKYIHS ANVLHRDLKP SNLLLNTTCD  160
LKICDFGLAR VADPDHDHTG FLTEYVATRW YRAPEIMLNS  200
KGYTKSIDIW SVGCILAEML SNRPIFPGKH YLDQLNHILG  240
ILGSPSQEDL NCIINLKARN YLLSLPHKNK VPWNRLFPNA  280
DSKALDLLDK MLTFNPHKRI EVEQALAHPY LEQYYDPSDE  320
PIAEAPFKFD MELDDLPKEK LKELIFEETA RFQPGYRS
```

Conf. (%)	Peptide Sequence	Pred. MW (Da)	Δmass
99	APEIMLNSK	1017.52	0.0001
99	FDMELDDLPK	1237.55	-0.0028
99	VADPDHDHTGFLTEYVATR	2143.00	0.0063
99	YIHSANVLHR	1208.65	0.0040
98	APTIEQMK	916.47	-0.0016
98	AAAAAAGPEMVR	1171.56	-0.0021

C

Name	Uniprot ID	Species	Score	%Cov	%Cov(50)	%Cov(95)	No. of Peptides (95%)
Erk2	P63085	Mus musculus	11.8	43.0	24.0	19.0	6
Grb2	Q60631	Mus musculus	11.6	45.2	41.9	36.4	7
Lyn	P25911	Mus musculus	8.7	24.6	10.7	10.7	5
TLR4	Q9QUK6	Mus musculus	6.0	15.9	4.6	4.6	3

Figure 2. Erk1/2 interacts with SCIMP

(A) GST-SCIMP-T1 coupled to GSH-Sepharose was used for pull-downs from LPS-activated (100 ng/mL) RAW 264.7 cell extracts. Bound proteins were separated by SDS-PAGE and visualized using colloidal Coomassie staining for gel excision. Excised bands were identified by liquid chromatography-mass spectrometry or mass spectrometry. A major band at ~42 kDa, absent from the GST control, was identified as Erk2.

(B) The sequence coverage of identified peptides in Erk2. Mass spectrometry analysis identified six independent trypsin-digested peptides from Erk2 with at least 98% confidence, including one peptide not found in Erk1. The predicted molecular mass of each peptide approximately matches with experimental molecular mass.

(C) Identified SCIMP binding partners. The mass spectrometry score is a measurement of peptide confidence from the ProteinPilot scoring algorithm: Score = −log(1 − (percent confidence/100)). %Cov (coverage) refers to the percentage of all identified peptide(s) relative to total amino acid sequence, whereas %Cov (50%) and %Cov (95%) refer to peptide coverage with 50% and 95% confidence, respectively. All peptides are identified from a single experiment.

SCIMP CRISPR-deleted RAW264.7 macrophages stably reconstituting exofacially-tagged Halo-SCIMP. In both LPS-stimulated (Figure 1A) and unstimulated cells (Figure 1B), Halo-SCIMP was localized on the cell surface, where it was enriched on filopodia and ruffles, and it was also present on vacuolar compartments inside cells. The addition of the fluid-phase marker 488-dextran 70 kDa, a specific marker for macropinosomes (Commisso et al., 2014), to the medium during imaging confirmed that SCIMP is on the membranes of large dextran-filled vacuolar macropinosomes that internalize from ruffles in response to LPS treatment (Figure 1A; Video S1). Imaging of unstimulated cells showed that SCIMP was predominantly localized to the cell surface and was also present on some smaller, constitutive, dextran-positive macropinosomes, indicating a lower level of SCIMP internalization under basal conditions. Its enrichment on ruffles and macropinosomes therefore positions SCIMP to participate in TLR signaling, and as a transmembrane adaptor, it is poised to recruit signaling molecules at these sites.

Erk1/2 is recruited to SCIMP downstream of TLR4

SCIMP scaffolds the Src kinase Lyn to recruit multiple effectors Grb2, Csk, and B-cell linker protein (BLNK)/SLP65, which bind to specific TLR-inducible phosphorylated tyrosine sites in the SCIMP cytoplasmic tail. SCIMP also potentiates MAPK signaling and the rapid activation of Erk1/2 downstream of TLR activation in macrophages (Luo et al., 2017, 2020; Figures S1B and S1C). As SCIMP itself does not possess intrinsic kinase activity, we hypothesized that SCIMP interactors must control downstream Erk1/2 signaling. To comprehensively identify additional SCIMP interactors and interrogate a possible relationship between SCIMP and Erk1/2, we performed an unbiased screen using a glutathione S-transferase (GST)-SCIMP cytoplasmic tail construct (T1) to pull-down binding partners from LPS-treated macrophage extracts (Figure 2A). Mass spectrometry analysis of pull-downs showed that, in addition to known SCIMP binding partners, including TLR4, Lyn, and Grb2, Erk2 itself is an unexpected SCIMP interactor based on its identification by six independent trypsin-digested peptides, each with over 95% confidence (Figures 2B and 2C).

The recruitment of Erk2 by SCIMP was then verified using affinity pull-downs and immunoprecipitations from RAW264.7 macrophage extracts (Figure 3). For affinity pull-downs, we used two truncated forms of the SCIMP cytoplasmic tail produced as GST fusion proteins: GST-SCIMP T1 comprising the
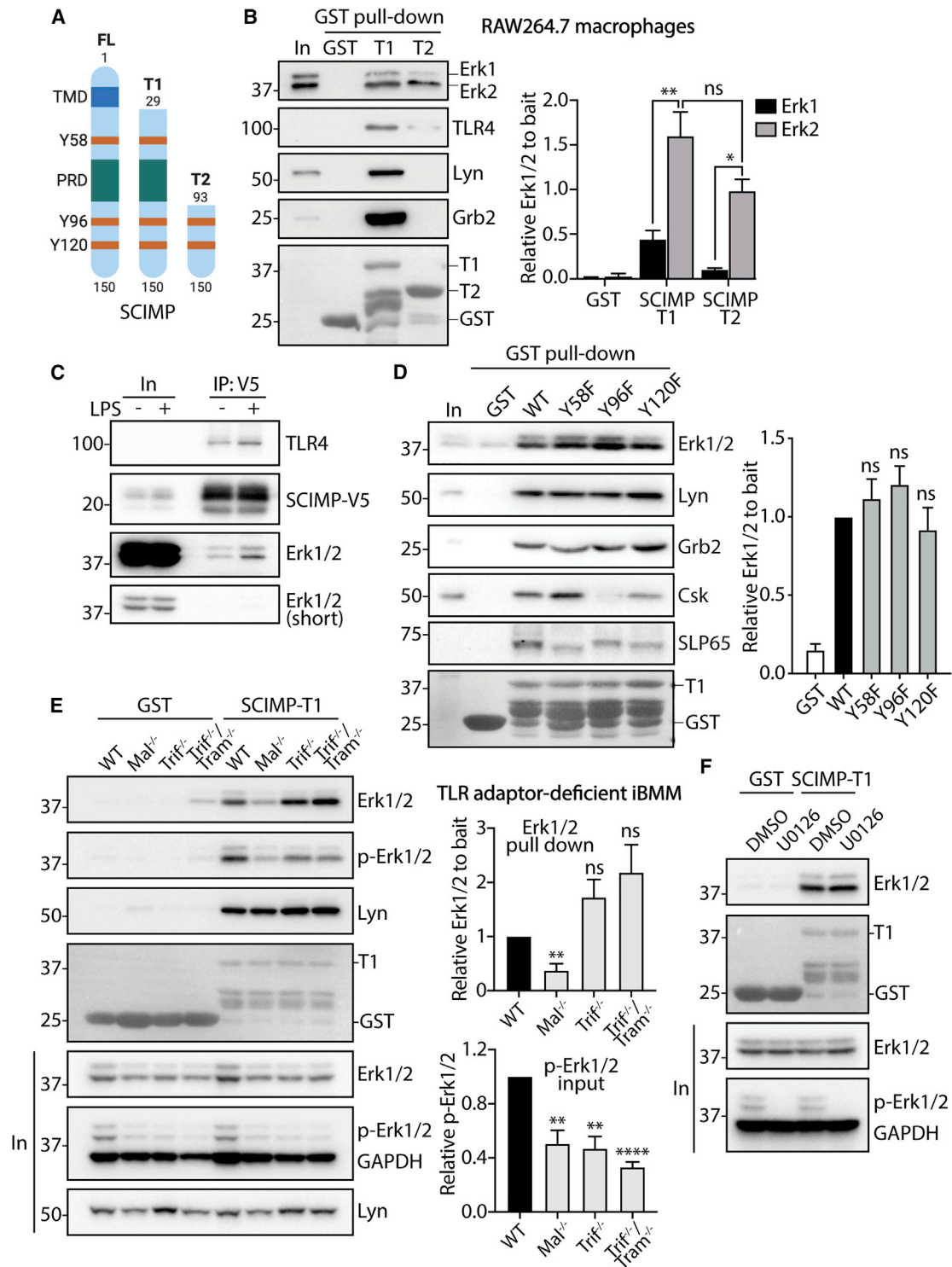
Figure 3. LPS promotes Erk1/2 recruitment to SCIMP

(A) SCIMP cytoplasmic domain constructs T1 (amino acids C29–F150) and truncation T2 (amino acids S93–F150). Created with BioRender.com.

(B) Bacterially expressed GST-SCIMP-T1 and GST-SCIMP-T2 were used to pull down Erk1/2 and other known binding partners (TLR4, Lyn, and Grb2) from LPS-stimulated (100 ng/mL) RAW264.7 cell lysates.

(C) CRISPR-Cas9-mediated SCIMP knockout RAW264.7 cells stably expressing V5-tagged WT SCIMP were treated ± 100 ng/mL LPS for 30 min, after which cell lysates were prepared, SCIMP-V5 was immunoprecipitated, and immunoblotting for Erk1/2 and TLR4 was performed.

(legend continued on next page)

entire intracellular region and GST-SCIMP T2 comprising the C-terminal region (Figure 3A). Both GST-SCIMP T1 and T2 were able to bind to Erk1/2 from LPS-activated macrophage extracts with statistical analyses showing no difference in Erk1/2 binding between T1 and T2 (Figure 3B). In contrast, endogenous TLR4 was pulled down by SCIMP-T1 more efficiently than SCIMP-T2, as previously reported (Luo et al., 2017). In addition, Grb2 and Lyn, which bind to phosphorylated Y58 and the proline-rich domain (PRD) of SCIMP, respectively, were selectively pulled down by only SCIMP-T1 as expected. This indicates that the C terminus of SCIMP, rather than Y58 or the PRD, is the primary binding site for Erk1/2 recruitment.

Next, CRISPR-mediated, SCIMP-deficient RAW264.7 cells reconstituted with recombinant V5-tagged SCIMP (Luo et al., 2017) were used to examine Erk1/2 binding in cells. Immunoprecipitation of SCIMP-V5 showed co-immunoprecipitation of Erk1/2 in addition to the known binding partner, TLR4 (Luo et al., 2017), with SCIMP/TLR4/Erk complex formation enhanced by LPS treatment (Figure 3C). SCIMP is rapidly phosphorylated by Lyn at Y58, Y96, and Y120 upon LPS stimulation (Luo et al., 2017). To examine whether any of these tyrosine residues regulate Erk1/2 binding, we used GST-tagged, site-specific phosphorylation-deficient SCIMP mutants (Y58F, Y96F, and Y120F). Affinity pull-downs with each of these mutants revealed no change in the binding of Erk1/2, suggesting that SCIMP phosphorylation at these three sites is not required for Erk1/2 recruitment in extracts from LPS-activated macrophages (Figure 3D). As controls for binding specificity, Lyn binding (at the PRD domain) was not affected by any of the tyrosine mutants, whereas Grb2, Csk, and SLP65 binding was reduced in Y58F-, Y96F-, or Y120F-expressing cells, respectively (Luo et al., 2017). Together, these results show that Erk1/2 is bound to the C-terminal tail of SCIMP, and this binding is enhanced in LPS-treated cells, but it does not involve LPS-induced phosphorylated tyrosines or indeed effectors recruited to these sites.

Unlike other TLRs, TLR4 signaling is mediated through all of the classical TLR adaptors MyD88, MAL, TRIF, and TRAM, which are required for downstream TPL2/MEK/Erk1/2 signaling (Banerjee et al., 2006; O'Neill and Bowie, 2007). Using a GST-SCIMP-T1 pull-down in Mal-, Trif-, or Trif/Tram-deficient immortalized mouse bone marrow-derived macrophages (iBMMs), we tested the requirement for these adaptors in the recruitment of Erk1/2 by SCIMP. As expected, SCIMP constitutively binds to Lyn, and this was unaffected in adaptor-deficient iBMMs. Notably, Mal was found to be required for the pull-down of Erk1/2 by SCIMP, although the absence of either Trif or Tram did not affect SCIMP-Erk binding (Figure 3E, upper). All adaptor-deficient cells showed a reduction in LPS-induced Erk1/2 phosphorylation in whole-cell lysates compared to wild-type (WT) cells (Figure 3E,

lower), as has been previously reported (Horng et al., 2002; Choi et al., 2010), indicating that activation of Erk1/2 itself is not required for its recruitment by SCIMP. This was confirmed by treatment with the MEK1/2 inhibitor U0126, which showed that SCIMP-Erk1/2 binding was unaffected by inhibition of Erk1/2 phosphorylation (Figure 3F). Therefore, Mal may act to bridge Erk1/2 recruitment to SCIMP, prior to its promotion of Erk1/2 activation in response to TLR4 stimulation.

SCIMP recruits Erk1/2 to membrane ruffles and macropinosomes

Erk1/2 is scaffolded by other proteins on specific membrane compartments in a variety of receptor-signaling pathways, including epidermal growth factor receptor (EGFR) signaling (Lavoie et al., 2020). In macrophages, Erk1/2 is generally a soluble kinase present throughout the cytoplasm, yet TLR signaling occurs on specific domains of the plasma membrane and macropinosomes and endosomes. As we showed that SCIMP is positioned at the TLR signaling sites on ruffles and macropinosomes and given its ability to bind to Erk2, we hypothesized that SCIMP may scaffold Erk2 at these sites for immune signaling. RAW264.7 macrophages co-expressing Halo-SCIMP and GFP-Erk2 were used for live imaging, which showed that, after addition of LPS, Erk2 can be recruited to membrane ruffles where SCIMP resides (Figure 4A). In line with its role in EGFR signaling, GFP-Erk2 also showed enrichment on membrane ruffles following epidermal growth factor (EGF) stimulation; however, Halo-SCIMP did not strongly localize to these sites, indicating that EGF-mediated membrane recruitment of Erk2 occurs independently of SCIMP. Ruffles and macropinosomes are highly dynamic membranes, and to characterize the spatiotemporal recruitment of Erk2 and SCIMP for TLR4 signaling, we performed high-speed, high-resolution, live-cell imaging of co-transfected, LPS-stimulated macrophages using lattice light-sheet microscopy (LLSM) (Condon et al., 2018). The resulting movies capture active ruffles that are enriched for both Halo-SCIMP and GFP-Erk2, giving rise to large, spherical macropinosomes, which were internalized (over ~1 min) with both SCIMP and Erk2 remaining attached to the limiting membrane of the newly closed macropinosome (Figure 4B; Video S2). A 2D slice depicts SCIMP-Erk2 colocalization on the dorsal ruffles and on internalized macropinosomes (Figure 4C; Video S3). The degree of colocalization in these regions was visualized as a ratiometric composite shown as a heatmap depicting intense convergence of Erk2 and SCIMP on the ruffles and newly formed macropinosomes, compared to "cooler" regions of the plasma membrane and other cellular compartments (Figures 4B and 4C; Videos S2, S3, and S4). This also highlights the acute, transient nature of Erk2 recruitment at these sites in response to LPS; cells without

---

(D) Representative immunoblot showing pull-down of GST-SCIMP-T1 WT, Y58F, Y96F, and Y120F in LPS-stimulated RAW264.7 cell lysates probed for Erk1/2, Lyn, Grb2, Csk, and SLP65.

(E) Representative immunoblot showing pull-down of GST-SCIMP-T1 in 100 ng/mL LPS-stimulated WT, $Mal^{-/-}$, $Trif^{-/-}$, and $Trif^{-/-}/Tram^{-/-}$ iBMMs probed for Erk1/2, phospho-Erk1/2 (Thr-202/Tyr-204), Lyn, and GAPDH (input samples).

(F) GST-SCIMP-T1 was used to pull down Erk1/2 from 100 ng/mL LPS-stimulated RAW264.7 cell lysates pre-treated with DMSO or 10 μM MEK1/2 inhibitor (U0126) for 1 h. Immunoblots were probed for Erk1/2, phospho-Erk1/2 (Thr-202/Tyr-204), and GAPDH.

Graphical data in (B), (D), and (E) (upper graph) show relative Erk1/2 levels normalized to bait or phospho-Erk1/2 normalized to GAPDH loading control in whole-cell lysates (lower graph) as mean+SEM from 3 independent experiments (n = 3), and statistical analysis was performed using one-way ANOVA with Sidak's multiple comparisons test (B) or Student's t test (D and E) (ns, non-significant; *p < 0.05; **p < 0.01; ****p < 0.0001).
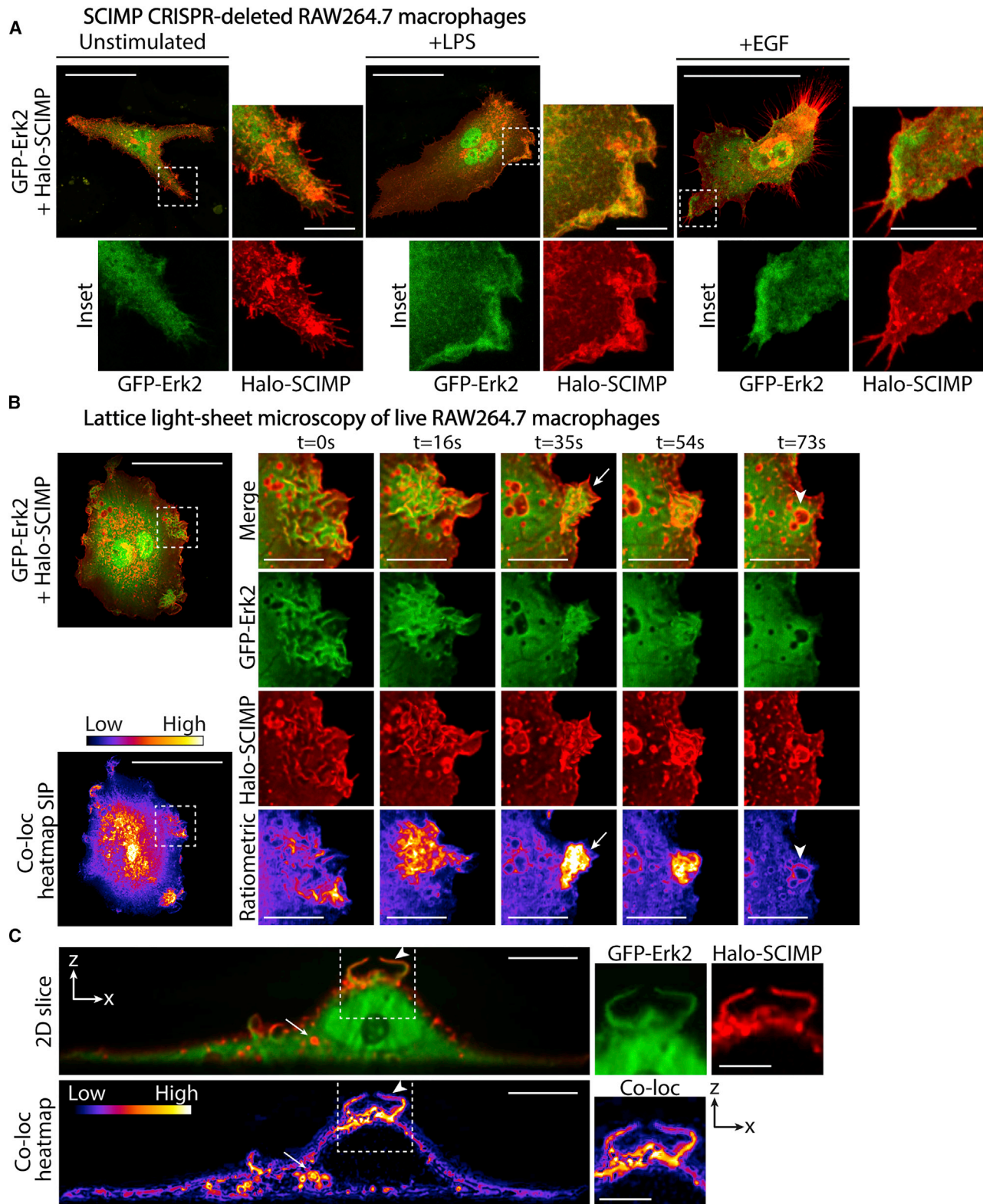
A   SCIMP CRISPR-deleted RAW264.7 macrophages

Unstimulated   +LPS   +EGF

GFP-Erk2 + Halo-SCIMP

Inset: GFP-Erk2   Halo-SCIMP   GFP-Erk2   Halo-SCIMP   GFP-Erk2   Halo-SCIMP

B   Lattice light-sheet microscopy of live RAW264.7 macrophages

GFP-Erk2 + Halo-SCIMP

Co-loc heatmap SIP   Low   High

t=0s   t=16s   t=35s   t=54s   t=73s

Merge
GFP-Erk2
Halo-SCIMP
Ratiometric

C

2D slice   z / x

Co-loc heatmap   Low   High

GFP-Erk2   Halo-SCIMP

Co-loc   z / x

Figure 4. Erk1/2 and SCIMP colocalize on ruffles and macropinosomes in response to LPS

(A) CRISPR-Cas9-mediated SCIMP knockout RAW264.7 cells expressing Halo-SCIMP (red) and GFP-Erk2 (green) with or without stimulation with 100 ng/mL LPS or 100 ng/mL EGF for 30 min. Scale bar: 50 μm (inset scale bar: 10 μm).

(legend continued on next page)

LPS stimulation showed reduced membrane colocalization of Erk2 and SCIMP (Video S5). These images demonstrate the co-localization of SCIMP and Erk2 on membrane domains, in keeping with their LPS-induced molecular interactions.

To determine whether SCIMP is required for the recruitment of Erk1/2 at membrane signaling sites, SCIMP-deleted RAW264.7 macrophages expressing GFP-Erk2 were imaged. These cells showed no enrichment of Erk2 at cell-surface ruffles induced by LPS stimulation; however, Erk2 recruitment to ruffles was then rescued by re-expression of Halo-SCIMP (Figure 5A). Affinity pull-down using the GST-tagged Toll/interleukin-1 receptor (TIR) domain of TLR4 in LPS-stimulated WT and *Scimp*$^{-/-}$ bone marrow-derived macrophages (BMMs) showed that the recruitment of Erk1/2 to TLR4 was significantly diminished in the absence of SCIMP (Figure 5B). Furthermore, immunoprecipitation of Erk1/2 from WT and *Scimp*$^{-/-}$ BMMs showed binding of TLR4 and Erk1/2 in WT BMMs, which was enhanced by LPS stimulation; however, no Erk1/2-TLR4 binding was detected in *Scimp*$^{-/-}$ BMMs, indicating that SCIMP is needed to scaffold Erk1/2 to activated TLR4 (Figure 5C). Together, these results pinpoint the cellular location of the SCIMP-Erk2 complex to sites on macrophage ruffles and macropinosomes, in response to TLR4 activation, and position SCIMP as a critical spatiotemporal scaffold for LPS-induced recruitment of Erk1/2 to these key TLR signaling sites.

SCIMP and Erk1/2 signaling for selective TLR-mediated cytokine production

The TPL2/Erk1/2 axis is known to promote both pro- and anti-inflammatory cytokine production downstream of activated TLRs, reflecting a broad role in cytokine programming for both the promotion and resolution of TLR-mediated inflammation (Banerjee et al., 2006). Erk1/2 regulates pro-inflammatory cytokines, including tumor necrosis factor (TNF), IL-6, and IL-1β (Flynn et al., 2019; Rousseau et al., 2008; Singh et al., 2016), as well as anti-inflammatory IL-10 (Sanin et al., 2015). Accordingly, BMMs treated with MEK1/2 inhibitor, U0126, showed decreased expression of these cytokines compared to untreated BMMs in response to LPS stimulation (Figure S2).

Although Erk1/2 signaling has a broad cytokine profile, SCIMP is selective in promoting a biased output of TLR-mediated pro-inflammatory cytokines IL-6 and IL-12p40 in macrophages, but not anti-inflammatory IL-10 or interferon β (IFNβ) (Luo et al., 2017). Given the recruitment and activation of Erk1/2 by SCIMP, we examined the production of Erk1/2-dependent cytokines in SCIMP-deficient BMMs activated with LPS. BMMs from both SCIMP homozygous (*Scimp*$^{-/-}$) and heterozygous (*Scimp*$^{+/-}$) knockout mice were deficient in the synthesis of TNF, IL-6, and IL-12p40, and of IL-1β, but not IL-10, compared to WT controls (*Scimp*$^{+/+}$) (Figure 6A). *Scimp*$^{+/-}$ BMMs expressed around 30% of the WT level of SCIMP, and yet the magnitude of the cytokine

defects was similar to those seen in *Scimp*$^{-/-}$ BMMs, suggesting that even a partial reduction in SCIMP expression impairs LPS-induced pro-inflammatory cytokine production. Consistently, *Scimp*$^{-/-}$ BMMs showed decreased secretion of TNF, IL-6, and IL-12p40 protein over a time course of 8 h and 24 h LPS treatment, and IL-10 secretion was unaffected by loss of SCIMP (Figure 6B). These findings were replicated after SCIMP silencing, where, in addition to IL-6 and IL-12p40 (Figure S3A), *Scimp* small interfering RNA (siRNA)-treated BMMs showed a reduction in LPS-induced IL-1β and TNF expression (Figure 6C). In addition to IL-10 and IFN-β, SCIMP silencing did not affect the expression of inflammatory chemokines CXCL10, CCL2, and CCL5 in response to LPS (Figure S3A). SCIMP deficiency therefore results in a specific defect in the pro-inflammatory arm of Erk1/2-mediated cytokine production downstream of TLR4 activation.
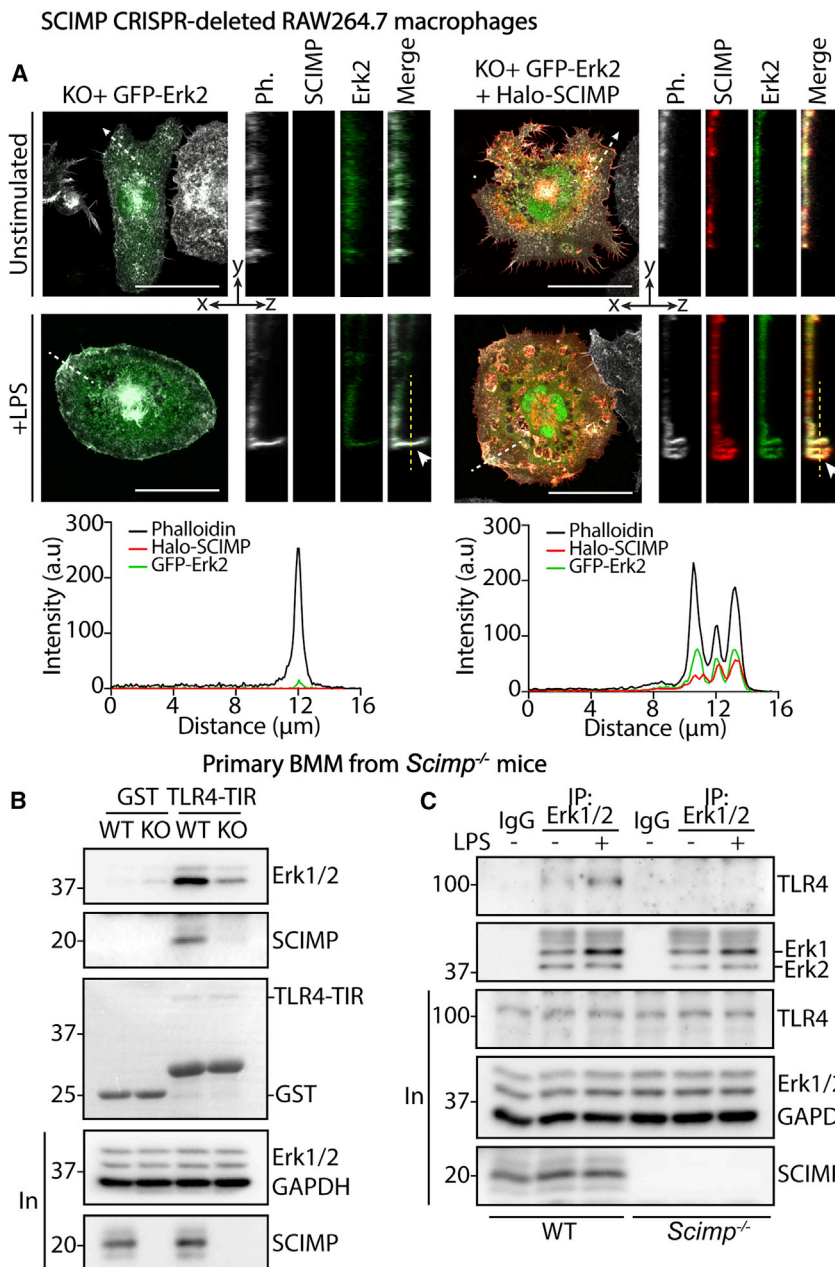
In promoting these selective effects on TLR-mediated cytokine production, it is important to note that expression of SCIMP itself is considerably upregulated by LPS activation (Figure S3B). Because SCIMP has close homologs within the pTRAP family, we examined the expression of Phosphoprotein associated with glycosphingolipid-enriched microdomains (PAG)/Csk-binding protein (CBP), Non-T cell activation linker (NTAL), and Linker for activation of T cells (LAT) in SCIMP-silenced BMMs, finding that all were unaffected by the loss of SCIMP (Figure S3C). BMMs from mice deficient in the closely related but non-myeloid specific pTRAP, PAG/CBP (*Cbp*$^{-/-}$), were stimulated with LPS, and the expression of pro-inflammatory cytokines TNF, IL-1β, and IL-12p40 was unaffected by loss of PAG/CBP, which was itself expressed at very low levels in BMMs (Figure S3D). Thus, SCIMP has a specific role in scaffolding Erk1/2, which results in a selective effect on LPS-induced pro-inflammatory cytokine expression. To further explore a mechanism for this selective induction downstream of TLRs, Erk1/2- and SCIMP-mediated transcriptional regulation was next explored.

Transcriptional regulation of cytokines through the SCIMP-Erk1/2 axis

TLR-induced cytokine production is transcriptionally regulated through the activity of inflammatory transcription factors, which directly activate or suppress target gene expression. Erk1/2 plays a role in NF-κB activation (Banerjee et al., 2006), and it phosphorylates AP-1 component c-Fos in TLR pathways (Brown et al., 2011; Chalmers et al., 2007; Gilley et al., 2009). BMMs treated with the upstream MEK1/2 inhibitor U0126 to abolish Erk1/2 signaling showed a significant dose-dependent reduction in c-Fos phosphorylation after LPS stimulation but showed no detectable change in NF-κB p65 phosphorylation compared to controls (Figure S4A). NF-κB phosphorylation promotes its pro-inflammatory transcriptional activity (Sasaki et al., 2005), and MAPK-mediated phosphorylation of AP-1 components

(B) Time series of 100 ng/mL LPS-treated RAW264.7 cell expressing Halo-SCIMP (red) and GFP-Erk2 (green) captured using LLSM. Colocalization of Halo-SCIMP and GFP-Erk2 computed from a sum intensity projection (SIP) using ImageJ and visualized using FireLUT is shown. Cell surface ruffles (arrows) and endosomes (arrowheads) are indicated. Scale bar: 50 μm (inset scale bar: 10 μm).

(C) x,z 2D reslice of a single frame from cell from (B) captured using LLSM. Colocalization of Halo-SCIMP (green) and GFP-Erk2 (red) computed using ImageJ and visualized using FireLUT is shown. Cell surface ruffles (arrowheads) and endosomes (arrows) are indicated. Scale bar: 10 μm (inset scale bar: 5 μm). Images from (A)–(C) are from independent experiments.

Figure 5. SCIMP is required for LPS-induced Erk1/2 localization at cell-surface ruffles and recruitment to TLR4

(A) Representative images of untreated and 100 ng/mL LPS-stimulated CRISPR-Cas9-mediated SCIMP knockout RAW264.7 cells expressing GFP-Erk2 (green) alone or in combination with Halo-SCIMP (red) and stained with phalloidin-647 (white). Z projections across the membrane (dashed white line) show dorsal surface ruffles after LPS treatment (arrowheads). Intensity profiles of ruffles quantified for individual channels are shown (yellow dashed line). Scale bar: 50 μm.

(B) Bacterially expressed GST-TLR4-TIR was used to pull down Erk1/2 from 100 ng/mL LPS-stimulated $Scimp^{+/+}$ and $Scimp^{-/-}$ BMM cell lysates and probed for Erk1/2, SCIMP, and GAPDH (input samples).

(C) Erk1/2 was immunoprecipitated from untreated and 30 min LPS-treated (100 ng/mL) WT and $Scimp^{-/-}$ BMMs, and immunoblots were probed for TLR4, Erk1/2, SCIMP, and GAPDH. Anti-human immunoglobulin G (IgG) was used as a negative immunoprecipitation control.

(B) and (C) are each representative of two independent experiments (n = 2).

c-Jun and c-Fos promote nuclear retention and transcriptional machinery complex formation for transcriptional activation (Karin, 1995; Li et al., 2004; Sasaki et al., 2006). Immunofluorescence imaging confirmed that MEK1/2 inhibition abolished nuclear localization of c-Fos in response to LPS and modestly reduced nuclear translocation of NF-κB p65 (Figures S4B and S5). This supports a role for Erk1/2-mediated promotion of c-Fos and NF-κB transcription factor activation downstream of TLR4.

We next examined the role of SCIMP in activation of a panel of Erk1/2-regulated transcription factors. Scimp-silenced BMMs (Figure 7A) showed a selective reduction in phosphorylation of

c-Fos, in contrast to c-Jun, within the AP-1 complex (Figure 7B), consistent with Erk1/2 phosphorylation of c-Fos. Additionally, there was a modest but significant reduction in NF-κB p65 phosphorylation in response to LPS after Scimp silencing, in line with an impairment of inhibitor of NF-κB (IκB) degradation reported previously (Luo et al., 2017). Erk1/2 has been shown to activate the transcription factor C/EBPβ in response to IFN-γ stimulation (Hu et al., 2001), but no such role downstream of TLRs has been described, and loss of SCIMP did not affect C/EBPβ activation following LPS stimulation (Figure 7B). Immunofluorescence analysis of c-Fos and NF-κB p65 nuclear translocation in LPS-treated $Scimp^{-/-}$ BMMs revealed reduced nuclear c-Fos at 60 min post-LPS treatment and a milder reduction in nuclear NF-κB p65 at both 15 and 60 min post-LPS compared to WT BMMs (Figures 7C and S5). Consistently, nuclear and cytoplasmic fractions from LPS-treated WT and $Scimp^{-/-}$ BMM lysates showed a marked reduction in both nuclear NF-κB p65 and c-Fos at 60 min post-LPS treatment in the absence of SCIMP (Figure 7D). Thus, these results mirror those obtained in MEK1/2 inhibitor-treated BMMs (Figure S4), indicating that SCIMP likely regulates c-Fos and NF-κB transcription factors through Erk1/2 signaling downstream of TLR4. The locale-specific recruitment of Erk1/2 by SCIMP thus provides a mechanism to drive transcription factor activation for the selective transcription of pro-inflammatory cytokines in TLR pathways.
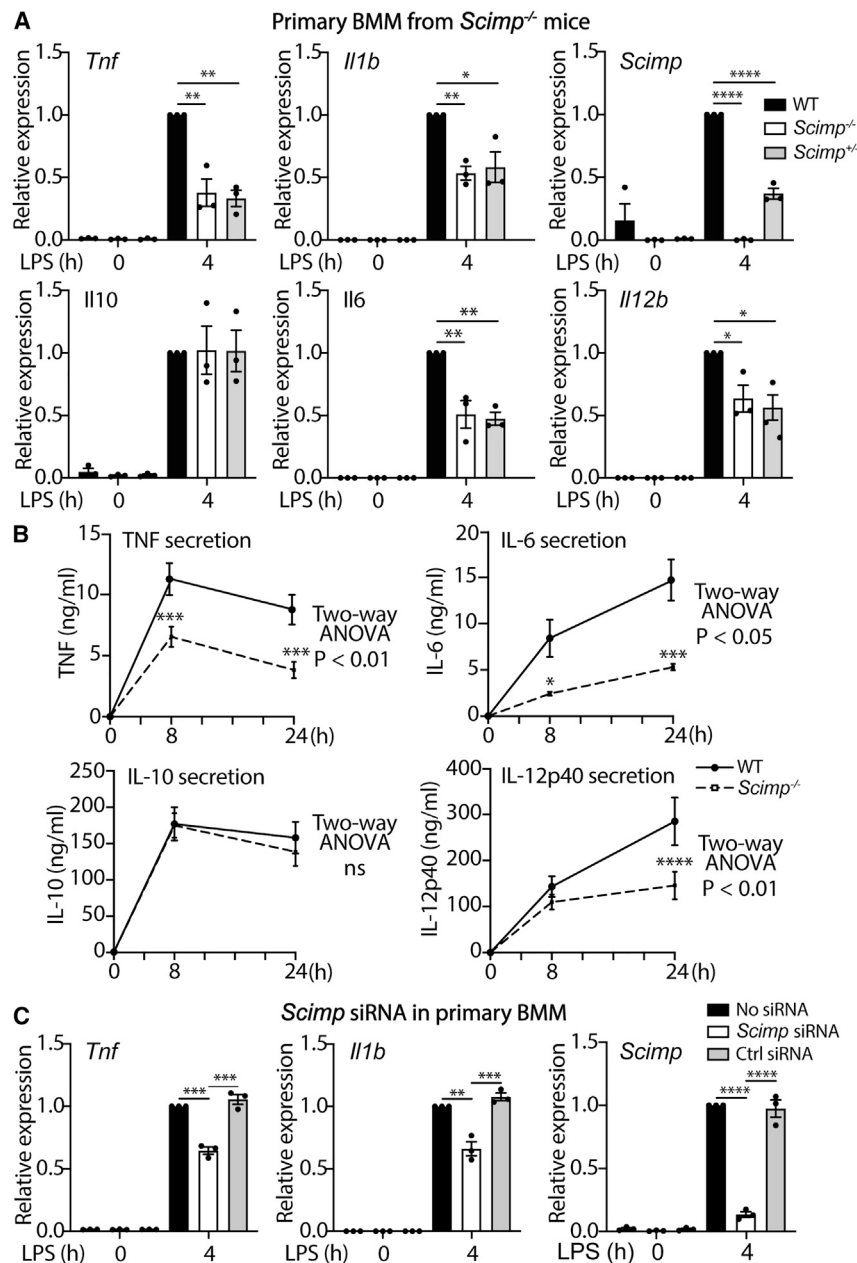
A

Primary BMM from *Scimp⁻ᐟ⁻* mice

B

C

Scimp siRNA in primary BMM

Figure 6. SCIMP promotes pro-inflammatory cytokine production in response to LPS

(A) BMMs from $Scimp^{+/+}$, $Scimp^{-/-}$, and $Scimp^{+/-}$ mice were stimulated with 100 ng/mL LPS for 4 h, and respective mRNA levels were analyzed by qRT-PCR and normalized relative to *Hprt*. Data are shown as mean+SEM for fold-change of $Scimp^{+/+}$ (4 h) from 3 independent experiments (n = 3), and statistical analysis was performed using one-way ANOVA with Sidak's multiple comparisons test (*p < 0.05; **p < 0.01; ****p < 0.0001).

(B) BMMs from $Scimp^{+/+}$ and $Scimp^{-/-}$ mice were stimulated with 100 ng/mL LPS for 8 h or 24 h, and levels of secreted TNF, IL-6, IL-10, and IL-12p40 were analyzed by ELISA. Data are shown as mean+SEM from n = 6 mice per genotype, and statistical analysis was performed using two-way ANOVA with Sidak's multiple comparisons test (*p < 0.05; ***p < 0.001; ****p < 0.0001).

(C) BMMs from wild-type mice were treated with *Scimp* siRNA, control siRNA, or no siRNA and cultured for 24 h before stimulation with 100 ng/mL LPS for 4 h. Respective mRNA levels were analyzed by qRT-PCR and normalized relative to *Hprt*. Data (relative to no siRNA 4 h LPS treatment) are shown as mean+SEM from 3 independent experiments (n = 3), and statistical analysis was performed using one-way ANOVA with Sidak's multiple comparisons test (**p < 0.01; ***p < 0.001; ****p < 0.0001).

Together, our results reveal Erk1/2 as a binding partner of SCIMP in macrophages and delineate a mechanism by which SCIMP recruits and scaffolds Erk1/2 to TLR4 at the cell membrane for c-Fos and NF-κB activation to selectively drive Erk1/2-mediated pro-inflammatory responses.

DISCUSSION

The transmembrane adaptor SCIMP has previously been characterized as a TLR adaptor in macrophages where it promotes specific pro-inflammatory cytokine production downstream of multiple TLRs (Luo et al., 2017, 2020). Mechanistically, we now show that SCIMP recruits and scaffolds Erk1/2 at key TLR4-signaling sites localized to membrane ruffles and macropinosomes, in an LPS-inducible manner. Using BMMs from $Scimp^{-/-}$ mice, previously used to characterize the role of SCIMP in dectin-1 signaling (Kralova et al., 2016), we show that a defect in LPS-induced pro-inflammatory cytokine expression is consistent with defective recruitment of Erk1/2 to TLR4 and impaired Erk1/2-mediated nuclear localization of c-Fos and NF-κB for transcriptional activation. Given the well-established roles of Erk1/2 in inflammatory responses downstream of TLRs, our results now address an unmet question of how Erk1/2 is spatiotemporally recruited for pro-inflammatory TLR signaling. We pose SCIMP as a key transmembrane scaffold for recruiting Erk1/2 to TLR4 to elicit a rapid, tailored pro-inflammatory response primarily through c-Fos and NF-κB activation (Figure S6).

In other cell-signaling pathways, Erk1/2 is generally recruited to RTKs by scaffolds that can bind multiple members of the classical Ras guanosine triphosphatase (GTPase)-MAPK signaling cascade, including Raf, MEK, and Erk (McKay and Morrison, 2007); however, these scaffolds are not known to be available in TLR settings. Ras activation can be promoted through Grb2/SOS complex formation and post-translational modification-dependent recruitment to specific cell membranes (Eisenberg and Henis, 2008). Although Grb2 is a known SCIMP effector,
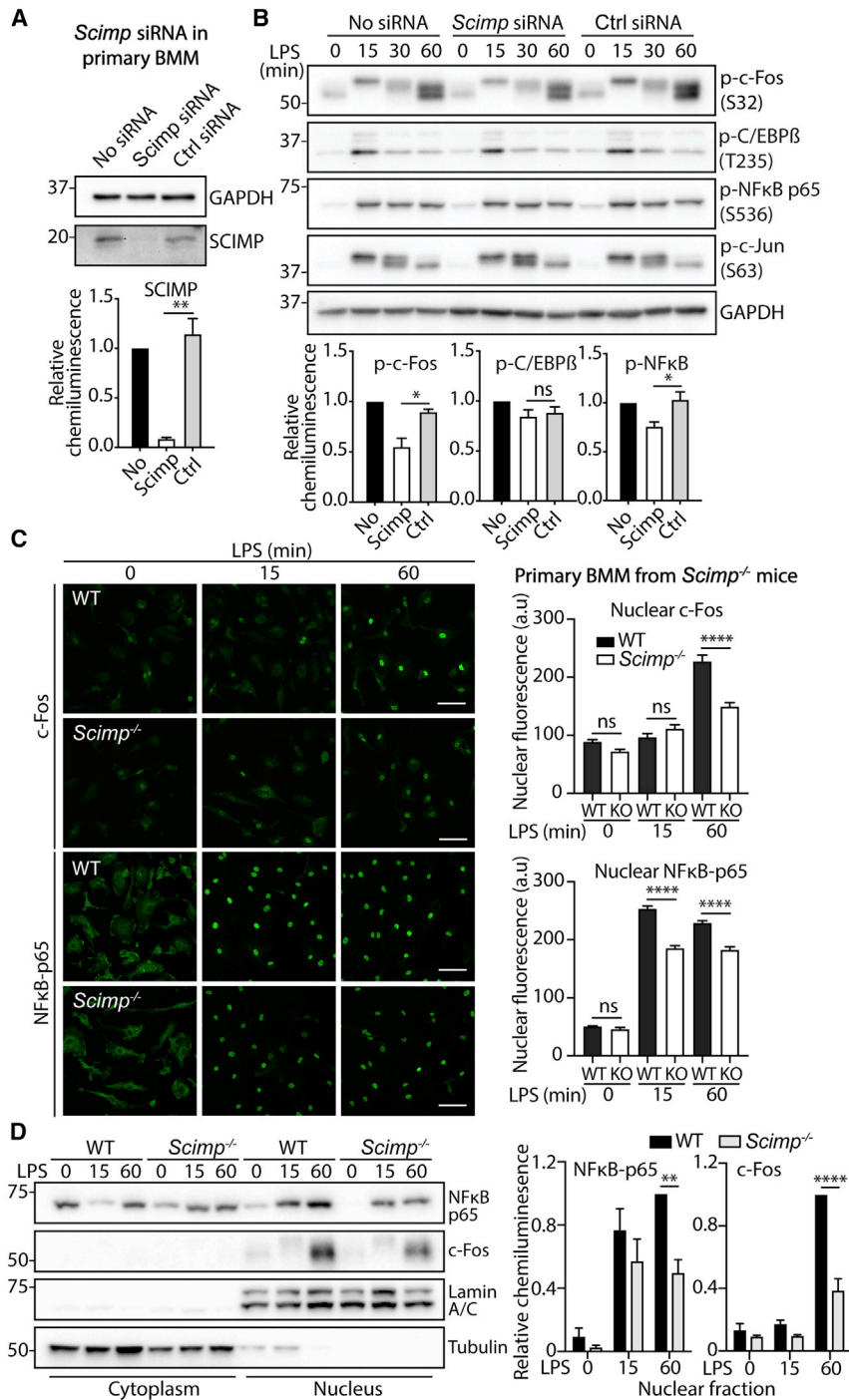
Previously, we showed that SCIMP can regulate activation of other MAPKs, including p38 and c-Jun N-terminal kinase (JNK), downstream of TLR4 (Luo et al., 2017). However, neither of these MAPKs was present in SCIMP pull-down experiments. Thus, the activation of p38 and JNK are likely to be mediated by other SCIMP effectors, such as the tyrosine family kinase, Lyn (Avila et al., 2012). SCIMP therefore appears to show selectivity as a scaffold, recruiting Erk1/2, but not other MAPKs. For Erk1/2, the selectivity of SCIMP as a scaffold for each of the Erk isoforms 1 and 2 remains more of an open question. Our mass spectrometry analysis identified Erk2, but not Erk1, as a SCIMP interactor, but subsequent SCIMP pull-downs detected both Erk isoforms. This may reflect the lower abundance of Erk1 compared to Erk2 in macrophage lysates (see Figure 3B), and so further studies are needed to resolve whether SCIMP has Erk isoform selectivity. Indeed, the redundancy of Erks1 and 2 has long been debated,

our results suggest that the LPS-inducible recruitment of Erk1/2 by SCIMP does not require the presence of Grb2, and we did not detect upstream kinases, such as TPL2, Raf, or MEK in our SCIMP pull-downs. The immune-specific scaffolding function of SCIMP was further demonstrated by the lack of SCIMP enrichment at sites of Erk2 membrane recruitment stimulated by EGF, a Ras-Raf-Grb2-SOS-dependent process, indicating that SCIMP is not implicated in EGFR-mediated Erk1/2 signaling.

and it may be that their relative abundance is a more prominent factor in determining Erk1/2 signaling (Buscà et al., 2016).

A feature of scaffolds is their ability to modulate the duration and amplitude of signaling (McKay and Morrison, 2007). Consistent with this, loss of SCIMP reduced the strength of the Erk1/2 signal at a single 15-min peak in our experiments. SCIMP can also promote sustained Erk1/2 activation downstream of MHC II and dectin-1 activation in B cells and DCs (Draber et al., 2011; Kralova et al., 2016). SCIMP is thus likely to coordinate Erk1/2 signaling from different immune receptors. pTRAPs exist clustered in lipid raft or TEM domains, along with multiple receptors, and different pTRAPs can play overlapping or redundant signaling roles (Curson et al., 2018). We examined the closely related pTRAP, PAG/CBP, which also scaffolds SCIMP effectors Lyn and Csk. Unlike SCIMP, PAG/CBP expression was not regulated by LPS in macrophages, and it did not control inflammatory cytokine production. Thus, SCIMP appears to be acting uniquely in this scaffolding capacity, as supported by recording defective pro-inflammatory cytokine responses in *Scimp*-deficient BMMs.

The cell surface ruffles and early macropinosomes that host TLR4 signaling in macrophages (Kagan et al., 2008; Luo et al., 2014a) are highly dynamic membrane environments. These locales are indeed well characterized as signaling hubs, enriched in actin polymerizing proteins, membrane phospholipids, lipid kinases, signaling kinases, and small G proteins with a high rate of turnover (Bohdanowicz et al., 2013; Swanson, 2008; Yoshida et al., 2009). Although signaling kinases, such as the pleckstrin homology (PH)-domain-containing Akt, are recruited by transient accumulation of PI(3,4,5)P$_3$ on early macropinosomes (Wall et al., 2019), Erk1/2 has no such membrane-targeting motif. This further highlights the requirement for a membrane-localized protein scaffold for Erk1/2 in TLR pathways. As a palmitoylated transmembrane protein, SCIMP is strategically positioned to recruit signaling kinases directly to the receptor complexes in lipid raft signaling domains. With the advent of high-resolution LLSM, it is possible to resolve distinct and highly dynamic membrane compartments and protein recruitment. Our ability to capture TLR4-induced enrichment of Erk1/2 with SCIMP at highly specific and dynamic sites on membranes graphically illustrates both the recruitment of a subset of the cytosolic Erk1/2 to ruffles and macropinosomes and the need for SCIMP as a scaffold at these sites. Thus, this spatiotemporal recruitment of Erk1/2 matches the compartmentalization of the SCIMP and Erk1/2-mediated signaling required to specifically generate pro-inflammatory responses.

In addition to IL-6 and IL-12p40, these data now show that SCIMP promotes the production of pro-inflammatory cytokines pro-IL-1β and TNF downstream of TLR4 stimulation in primary macrophages. Following TLR-induced expression, IL-1β is released by innate immune cells in its mature form following activation of the inflammasome multimeric protein complex, which leads to pro-IL-1β cleavage, induction of pyroptotic inflammatory cell death, and secretion of mature IL-1β (Chan and Schroder, 2020). Recently, a key role for SCIMP in alternative inflammasome activation has emerged. In addition to scaffolding Lyn for TLR and B cell receptor signaling (Draber et al., 2011; Luo et al., 2017), SCIMP additionally recruits Syk kinase for caspase-8-dependent NLRP3 inflammasome assembly and mature

IL-1β secretion downstream of TLR2/4 (Zewinger et al., 2020). Complementary to these findings, we show that SCIMP promotes the Erk1/2-mediated expression of pro-IL-1β downstream of TLR4, thereby underlining the importance of the SCIMP as a crucial multi-level regulator of IL-1β production in macrophages. Distinct to its role in promotion of TLR-induced pro-IL-1β expression, Erk1/2 signaling also plays an important role in NLRP3 inflammasome priming (D'Espessailles et al., 2018; Ghonime et al., 2014). Therefore, it remains to be seen whether SCIMP is also an Erk1/2 scaffold in inflammasome activation pathways.

In TLR pathways, the kinase TPL2 acts downstream of multiple TLR adaptors, including MyD88/MAL and TRIF/TRAM for activation of MEK/Erk and c-Fos for inflammatory output, including control of TRIF-dependent IFN-β and IL-10 production (Banerjee et al., 2006; Kaiser et al., 2009). In line with this, we show that activity of the TPL2 downstream kinase MEK1/2 is essential for Erk1/2 phosphorylation and c-Fos activation. MEK1/2 inhibition abolishes both MyD88-dependent pro-inflammatory and TRIF-dependent type I interferon genes downstream of TLR4. However, SCIMP does not control Erk1/2-dependent IL-10 and IFN-β production. Thus, our data suggest that a subset of Erk1/2 scaffolded by SCIMP selectively drives only the pro-inflammatory signaling branch downstream of TLR4. Interestingly, the recruitment of Erk1/2 by SCIMP is dependent on surface TLR4 adaptor Mal, but not on endosomal TLR4 adaptors TRIF or TRAM (Figure 3E). It may be that endosomal TLR adaptors utilize an alternative signaling adaptor for Erk1/2 recruitment and activation downstream of TLR4 for type I interferon production. Therefore, our data are consistent with SCIMP acting at the surface for TLR4 signaling, highlighting an interesting segregation of Erk1/2 activation between MyD88-dependent surface and TRIF-dependent endosomal TLR4 signaling.

The promotion of c-Fos and NF-κB activation by SCIMP in response to LPS is concurrent with the role of these potent transcription factors in inflammatory cytokine production. The specific regulation of Erk1/2-mediated c-Fos activation within the AP-1 complex, but not c-Jun, which is primarily regulated by the MAPK JNK (Ip and Davis, 1998), points to the specificity of the SCIMP inflammatory response. Although the AP-1 complex is a key pro-inflammatory modulator (Shaulian and Karin, 2002), macrophages from c-Fos-deficient mice conversely display increased production of TNF, IL-6, and IL-12p40 in response to LPS, which can be attributed to upregulated NF-κB expression (Ray et al., 2006). NF-κB and AP-1 can be simultaneously activated by the same stimuli and show synergistic cross-talk for enhanced gene expression (Stein et al., 1993), and NF-κB regulates c-Fos expression and AP-1 activation through Elk-1 and MAPK signaling (Fujioka et al., 2004). In addition to c-Fos, Erk1/2 can activate NF-κB through IκB kinase (IKK) (Chen and Lin, 2001; Eliopoulos et al., 2003; Kawai and Akira, 2007). Hence, interplay between SCIMP-mediated c-Fos and NF-κB activation through Erk1/2 may provide a further means to tailor specific pro-inflammatory output downstream of TLR4.

Finally, TLR signaling dysfunction is associated with the pathogenesis of autoimmune diseases (Barrat et al., 2005; Broen et al., 2012), many of which display MAPK/Erk1/2 dysregulation (Arthur and Ley, 2013; Gorelik and Richardson, 2010; Thalhamer

et al., 2008) and perturbed levels of pro-inflammatory cytokines (Hirano et al., 1988; Linker-Israeli et al., 1991; Liu et al., 1999; Turner et al., 2014). SCIMP is genetically linked to a range of inflammatory and autoimmune diseases, such as systemic lupus erythematosus (SLE), rheumatoid arthritis (RA) (Dozmorov et al., 2014), as well as Alzheimer's disease (AD) (Jansen et al., 2019; Lambert et al., 2013; Liu et al., 2017; Luo et al., 2019; Moreno-Grau et al., 2019) and its inherent innate immune dysfunction (Heneka et al., 2015a, 2015b). SCIMP regulation of disease-associated pro-inflammatory cytokines through the pro-inflammatory arm of Erk1/2 signaling may therefore provide an axis amenable to therapeutic intervention in inflammation-related diseases.

STAR★METHODS

Detailed methods are provided in the online version of this paper and include the following:

- KEY RESOURCES TABLE
- RESOURCE AVAILABILITY
  - Lead contact
  - Materials availability
  - Data and code availability
- EXPERIMENTAL MODEL AND SUBJECT DETAILS
  - Animals
  - Cell lines
  - Bacterial Strains
  - Ethics statement
- METHOD DETAILS
  - Generation of DNA constructs and protein expression
  - siRNA-mediated gene silencing and DNA transfection
  - Immunoblotting
  - Affinity pull down and co-immunoprecipitation
  - Mass spectrometry
  - Gene expression and cytokine analysis
  - Immunofluorescence & fixed cell imaging
  - Live cell imaging of dextran uptake
  - Lattice light sheet live cell imaging
- QUANTIFICATION AND STATISTICAL ANALYSIS
  - Image analysis
  - Statistics

SUPPLEMENTAL INFORMATION

Supplemental information can be found online at https://doi.org/10.1016/j.celrep.2021.109662.

REFERENCES

Akira, S., and Takeda, K. (2004). Toll-like receptor signalling. Nat. Rev. Immunol. 4, 499–511.

An, H., Yu, Y., Zhang, M., Xu, H., Qi, R., Yan, X., Liu, S., Wang, W., Guo, Z., Guo, J., et al. (2002). Involvement of ERK, p38 and NF-kappaB signal transduction in regulation of TLR2, TLR4 and TLR9 gene expression induced by lipopolysaccharide in mouse dendritic cells. Immunology 106, 38–45.

Arthur, J.S.C., and Ley, S.C. (2013). Mitogen-activated protein kinases in innate immunity. Nat. Rev. Immunol. 13, 679–692.

Avila, M., Martinez-Juarez, A., Ibarra-Sanchez, A., and Gonzalez-Espinosa, C. (2012). Lyn kinase controls TLR4-dependent IKK and MAPK activation modulating the activity of TRAF-6/TAK-1 protein complex in mast cells. Innate Immun. 18, 648–660.

Banerjee, A., Gugasyan, R., McMahon, M., and Gerondakis, S. (2006). Diverse Toll-like receptors utilize Tpl2 to activate extracellular signal-regulated kinase (ERK) in hemopoietic cells. Proc. Natl. Acad. Sci. USA 103, 3274–3279.

Barrat, F.J., Meeker, T., Gregorio, J., Chan, J.H., Uematsu, S., Akira, S., Chang, B., Duramad, O., and Coffman, R.L. (2005). Nucleic acids of mammalian origin can act as endogenous ligands for Toll-like receptors and may promote systemic lupus erythematosus. J. Exp. Med. 202, 1131–1139.

Bohdanowicz, M., Schlam, D., Hermansson, M., Rizzuti, D., Fairn, G.D., Ueyama, T., Somerharju, P., Du, G., and Grinstein, S. (2013). Phosphatidic acid is required for the constitutive ruffling and macropinocytosis of phagocytes. Mol. Biol. Cell 24, 1700–1712, S1–S7.

Broen, J.C.A., Bossini-Castillo, L., van Bon, L., Vonk, M.C., Knaapen, H., Beretta, L., Rueda, B., Hesselstrand, R., Herrick, A., Worthington, J., et al.; Spanish Systemic Sclerosis Group (2012). A rare polymorphism in the gene for Toll-like receptor 2 is associated with systemic sclerosis phenotype and increases the production of inflammatory mediators. Arthritis Rheum. 64, 264–271.

Brown, J., Wang, H., Hajishengallis, G.N., and Martin, M. (2011). TLR-signaling networks: an integration of adaptor molecules, kinases, and cross-talk. J. Dent. Res. 90, 417–427.

Buscà, R., Pouysségur, J., and Lenormand, P. (2016). ERK1 and ERK2 map kinases: specific roles or functional redundancy? Front. Cell Dev. Biol. 4, 53.

Casar, B., and Crespo, P. (2016). ERK signals: scaffolding scaffolds? Front. Cell Dev. Biol. 4, 49.

Chalmers, C.J., Gilley, R., March, H.N., Balmanno, K., and Cook, S.J. (2007). The duration of ERK1/2 activity determines the activation of c-Fos and Fra-1

and the composition and quantitative transcriptional output of AP-1. Cell. Signal. *19*, 695–704.

Chan, A.H., and Schroder, K. (2020). Inflammasome signaling and regulation of interleukin-1 family cytokines. J. Exp. Med. *217*, e20190314.

Chen, B.-C., and Lin, W.-W. (2001). PKC- and ERK-dependent activation of I κ B kinase by lipopolysaccharide in macrophages: enhancement by P2Y receptor-mediated CaMK activation. Br. J. Pharmacol. *134*, 1055–1065.

Choi, Y.J., Im, E., Chung, H.K., Pothoulakis, C., and Rhee, S.H. (2010). TRIF mediates Toll-like receptor 5-induced signaling in intestinal epithelial cells. J. Biol. Chem. *285*, 37570–37578.

Commisso, C., Flinn, R.J., and Bar-Sagi, D. (2014). Determining the macropinocytic index of cells through a quantitative image-based assay. Nat. Protoc. *9*, 182–192.

Condon, N.D., Heddleston, J.M., Chew, T.-L., Luo, L., McPherson, P.S., Ioannou, M.S., Hodgson, L., Stow, J.L., and Wall, A.A. (2018). Macropinosome formation by tent pole ruffling in macrophages. J. Cell Biol. *217*, 3873–3885.

Curson, J.E.B., Luo, L., Sweet, M.J., and Stow, J.L. (2018). pTRAPs: transmembrane adaptors in innate immune signaling. J. Leukoc. Biol. Published March 30, 2018. https://doi.org/10.1002/JLB.2RI1117-474R.

D'Espessailles, A., Mora, Y.A., Fuentes, C., and Cifuentes, M. (2018). Calcium-sensing receptor activates the NLRP3 inflammasome in LS14 preadipocytes mediated by ERK1/2 signaling. J. Cell. Physiol. *233*, 6232–6240.

Dozmorov, M.G., Wren, J.D., and Alarcón-Riquelme, M.E. (2014). Epigenomic elements enriched in the promoters of autoimmunity susceptibility genes. Epigenetics *9*, 276–285.

Draber, P., Vonkova, I., Stepanek, O., Hrdinka, M., Kucova, M., Skopcova, T., Otahal, P., Angelisova, P., Horejsi, V., Yeung, M., et al. (2011). SCIMP, a transmembrane adaptor protein involved in major histocompatibility complex class II signaling. Mol. Cell. Biol. *31*, 4550–4562.

Dumitru, C.D., Ceci, J.D., Tsatsanis, C., Kontoyiannis, D., Stamatakis, K., Lin, J.H., Patriotis, C., Jenkins, N.A., Copeland, N.G., Kollias, G., and Tsichlis, P.N. (2000). TNF-alpha induction by LPS is regulated posttranscriptionally via a Tpl2/ERK-dependent pathway. Cell *103*, 1071–1083.

Eisenberg, S., and Henis, Y.I. (2008). Interactions of Ras proteins with the plasma membrane and their roles in signaling. Cell. Signal. *20*, 31–39.

Eliopoulos, A.G., Wang, C.-C., Dumitru, C.D., and Tsichlis, P.N. (2003). Tpl2 transduces CD40 and TNF signals that activate ERK and regulates IgE induction by CD40. EMBO J. *22*, 3855–3864.

Flynn, C.M., Garbers, Y., Lokau, J., Wesch, D., Schulte, D.M., Laudes, M., Lieb, W., Aparicio-Siegmund, S., and Garbers, C. (2019). Activation of Toll-like receptor 2 (TLR2) induces interleukin-6 trans-signaling. Sci. Rep. *9*, 7306.

Fujioka, S., Niu, J., Schmidt, C., Sclabas, G.M., Peng, B., Uwagawa, T., Li, Z., Evans, D.B., Abbruzzese, J.L., and Chiao, P.J. (2004). NF-kappaB and AP-1 connection: mechanism of NF-kappaB-dependent regulation of AP-1 activity. Mol. Cell. Biol. *24*, 7806–7819.

Ghonime, M.G., Shamaa, O.R., Das, S., Eldomany, R.A., Fernandes-Alnemri, T., Alnemri, E.S., Gavrilin, M.A., and Wewers, M.D. (2014). Inflammasome priming by lipopolysaccharide is dependent upon ERK signaling and proteasome function. J. Immunol. *192*, 3881–3888.

Gilley, R., March, H.N., and Cook, S.J. (2009). ERK1/2, but not ERK5, is necessary and sufficient for phosphorylation and activation of c-Fos. Cell. Signal. *21*, 969–977.

Gorelik, G., and Richardson, B. (2010). Key role of ERK pathway signaling in lupus. Autoimmunity *43*, 17–22.

Heneka, M.T., Golenbock, D.T., and Latz, E. (2015a). Innate immunity in Alzheimer's disease. Nat. Immunol. *16*, 229–236.

Heneka, M.T., Carson, M.J., El Khoury, J., Landreth, G.E., Brosseron, F., Feinstein, D.L., Jacobs, A.H., Wyss-Coray, T., Vitorica, J., Ransohoff, R.M., et al. (2015b). Neuroinflammation in Alzheimer's disease. Lancet Neurol. *14*, 388–405.

Hirano, T., Matsuda, T., Turner, M., Miyasaka, N., Buchan, G., Tang, B., Sato, K., Shimizu, M., Maini, R., Feldmann, M., et al. (1988). Excessive production of interleukin 6/B cell stimulatory factor-2 in rheumatoid arthritis. Eur. J. Immunol. *18*, 1797–1801.

Horejsí, V., Zhang, W., and Schraven, B. (2004). Transmembrane adaptor proteins: organizers of immunoreceptor signalling. Nat. Rev. Immunol. *4*, 603–616.

Horng, T., Barton, G.M., Flavell, R.A., and Medzhitov, R. (2002). The adaptor molecule TIRAP provides signalling specificity for Toll-like receptors. Nature *420*, 329–333.

Hu, J., Roy, S.K., Shapiro, P.S., Rodig, S.R., Reddy, S.P.M., Platanias, L.C., Schreiber, R.D., and Kalvakolanu, D.V. (2001). ERK1 and ERK2 activate CCAAAT/enhancer-binding protein-β-dependent gene transcription in response to interferon-γ. J. Biol. Chem. *276*, 287–297.

Ip, Y.T., and Davis, R.J. (1998). Signal transduction by the c-Jun N-terminal kinase (JNK)–from inflammation to development. Curr. Opin. Cell Biol. *10*, 205–219.

Jansen, I.E., Savage, J.E., Watanabe, K., Bryois, J., Williams, D.M., Steinberg, S., Sealock, J., Karlsson, I.K., Hägg, S., Athanasiu, L., et al. (2019). Genome-wide meta-analysis identifies new loci and functional pathways influencing Alzheimer's disease risk. Nat. Genet. *51*, 404–413.

Kagan, J.C., Su, T., Horng, T., Chow, A., Akira, S., and Medzhitov, R. (2008). TRAM couples endocytosis of Toll-like receptor 4 to the induction of interferon-β. Nat. Immunol. *9*, 361–368.

Kaiser, F., Cook, D., Papoutsopoulou, S., Rajsbaum, R., Wu, X., Yang, H.-T., Grant, S., Ricciardi-Castagnoli, P., Tsichlis, P.N., Ley, S.C., and O'Garra, A. (2009). TPL-2 negatively regulates interferon-β production in macrophages and myeloid dendritic cells. J. Exp. Med. *206*, 1863–1871.

Karin, M. (1995). The regulation of AP-1 activity by mitogen-activated protein kinases. J. Biol. Chem. *270*, 16483–16486.

Kawai, T., and Akira, S. (2007). Signaling to NF-kappaB by Toll-like receptors. Trends Mol. Med. *13*, 460–469.

Kralova, J., Fabisik, M., Pokorna, J., Skopcova, T., Malissen, B., and Brdicka, T. (2016). The transmembrane adaptor protein SCIMP facilitates sustained dectin-1 signaling in dendritic cells. J. Biol. Chem. *291*, 16530–16540.

Kuriakose, T., Rada, B., and Watford, W.T. (2014). Tumor progression locus 2-dependent oxidative burst drives phosphorylation of extracellular signal-regulated kinase during TLR3 and 9 signaling. J. Biol. Chem. *289*, 36089–36100.

Lambert, J.C., Ibrahim-Verbaas, C.A., Harold, D., Naj, A.C., Sims, R., Bellenguez, C., DeStafano, A.L., Bis, J.C., Beecham, G.W., Grenier-Boley, B., et al.; European Alzheimer's Disease Initiative (EADI); Genetic and Environmental Risk in Alzheimer's Disease; Alzheimer's Disease Genetic Consortium; Cohorts for Heart and Aging Research in Genomic Epidemiology (2013). Meta-analysis of 74,046 individuals identifies 11 new susceptibility loci for Alzheimer's disease. Nat. Genet. *45*, 1452–1458.

Lavoie, H., Gagnon, J., and Therrien, M. (2020). ERK signalling: a master regulator of cell behaviour, life and fate. Nat. Rev. Mol. Cell Biol. *21*, 607–632.

Li, L., Feng, Z., and Porter, A.G. (2004). JNK-dependent phosphorylation of c-Jun on serine 63 mediates nitric oxide-induced apoptosis of neuroblastoma cells. J. Biol. Chem. *279*, 4058–4065.

Linker-Israeli, M., Deans, R.J., Wallace, D.J., Prehn, J., Ozeri-Chen, T., and Klinenberg, J.R. (1991). Elevated levels of endogenous IL-6 in systemic lupus erythematosus. A putative role in pathogenesis. J. Immunol. *147*, 117–123.

Liu, T.F., Jones, B.M., Wong, R.W., and Srivastava, G. (1999). Impaired production of IL-12 in systemic lupus erythematosus. III: deficient IL-12 p40 gene expression and cross-regulation of IL-12, IL-10 and IFN-gamma gene expression. Cytokine *11*, 805–811.

Liu, J.Z., Erlich, Y., and Pickrell, J.K. (2017). Case-control association mapping by proxy using family history of disease. Nat. Genet. *49*, 325–331.

Lu, Y.-C., Kim, I., Lye, E., Shen, F., Suzuki, N., Suzuki, S., Gerondakis, S., Akira, S., Gaffen, S.L., Yeh, W.-C., and Ohashi, P.S. (2009). Differential role for c-Rel and C/EBPbeta/δ in TLR-mediated induction of proinflammatory cytokines. J. Immunol. *182*, 7212–7221.

Luo, L., Wall, A.A., Yeo, J.C., Condon, N.D., Norwood, S.J., Schoenwaelder, S., Chen, K.W., Jackson, S., Jenkins, B.J., Hartland, E.L., et al. (2014a).

Rab8a interacts directly with PI3Kγ to modulate TLR4-driven PI3K and mTOR signalling. Nat. Commun. 5, 4407.

Luo, L., King, N.P., Yeo, J.C., Jones, A., and Stow, J.L. (2014b). Single-step protease cleavage elution for identification of protein-protein interactions from GST pull-down and mass spectrometry. Proteomics 14, 19–23.

Luo, L., Bokil, N.J., Wall, A.A., Kapetanovic, R., Lansdaal, N.M., Marceline, F., Burgess, B.J., Tong, S.J., Guo, Z., Alexandrov, K., et al. (2017). SCIMP is a transmembrane non-TIR TLR adaptor that promotes proinflammatory cytokine production from macrophages. Nat. Commun. 8, 14133.

Luo, L., Lucas, R.M., Liu, L., and Stow, J.L. (2019). Signalling, sorting and scaffolding adaptors for Toll-like receptors. J. Cell Sci. 133, jcs239194.

Luo, L., Curson, J.E.B., Liu, L., Wall, A.A., Tuladhar, N., Lucas, R.M., Sweet, M.J., and Stow, J.L. (2020). SCIMP is a universal Toll-like receptor adaptor in macrophages. J. Leukoc. Biol. 107, 251–262.

McKay, M.M., and Morrison, D.K. (2007). Integrating signals from RTKs to ERK/MAPK. Oncogene 26, 3113–3121.

Medzhitov, R. (2001). Toll-like receptors and innate immunity. Nat. Rev. Immunol. 1, 135–145.

Moreno-Grau, S., de Rojas, I., Hernández, I., Quintela, I., Montrreal, L., Alegret, M., Hernández-Olasagarre, B., Madrid, L., González-Perez, A., Maroñas, O., et al.; GR@ACE consortium; DEGESCO consortium; Alzheimer's Disease Neuroimaging Initiative (2019). Genome-wide association analysis of dementia and its clinical endophenotypes reveal novel loci associated with Alzheimer's disease and three causality networks: the GR@ACE project. Alzheimers Dement. 15, 1333–1347.

O'Neill, L.A.J., and Bowie, A.G. (2007). The family of five: TIR-domain-containing adaptors in Toll-like receptor signalling. Nat. Rev. Immunol. 7, 353–364.

Ogata, T., Naito, D., Nakanishi, N., Hayashi, Y.K., Taniguchi, T., Miyagawa, K., Hamaoka, T., Maruyama, N., Matoba, S., Ikeda, K., et al. (2014). MURC/Cavin-4 facilitates recruitment of ERK to caveolae and concentric cardiac hypertrophy induced by α1-adrenergic receptors. Proc. Natl. Acad. Sci. USA 111, 3811–3816.

Ray, N., Kuwahara, M., Takada, Y., Maruyama, K., Kawaguchi, T., Tsubone, H., Ishikawa, H., and Matsuo, K. (2006). c-Fos suppresses systemic inflammatory response to endotoxin. Int. Immunol. 18, 671–677.

Rousseau, S., Papoutsopoulou, M., Symons, A., Cook, D., Lucocq, J.M., Prescott, A.R., O'Garra, A., Ley, S.C., and Cohen, P. (2008). TPL2-mediated activation of ERK1 and ERK2 regulates the processing of pre-TNF α in LPS-stimulated macrophages. J. Cell Sci. 121, 149–154.

Sanin, D.E., Prendergast, C.T., and Mountford, A.P. (2015). IL-10 production in macrophages is regulated by a TLR-driven CREB-mediated mechanism that is linked to genes involved in cell metabolism. J. Immunol. 195, 1218–1232.

Sasaki, C.Y., Barberi, T.J., Ghosh, P., and Longo, D.L. (2005). Phosphorylation of RelA/p65 on serine 536 defines an IκBα-independent NF-κB pathway. J. Biol. Chem. 280, 34538–34547.

Sasaki, T., Kojima, H., Kishimoto, R., Ikeda, A., Kunimoto, H., and Nakajima, K. (2006). Spatiotemporal regulation of c-Fos by ERK5 and the E3 ubiquitin ligase UBR1, and its biological role. Mol. Cell 24, 63–75.

Schindelin, J., Arganda-Carreras, I., Frise, E., Kaynig, V., Longair, M., Pietzsch, T., Preibisch, S., Rueden, C., Saalfeld, S., Schmid, B., et al. (2012). Fiji: an open-source platform for biological-image analysis. Nat. Methods 9, 676–682.

Schmitz, F., Heit, A., Guggemoos, S., Krug, A., Mages, J., Schiemann, M., Adler, H., Drexler, I., Haas, T., Lang, R., and Wagner, H. (2007). Interferon-regulatory-factor 1 controls Toll-like receptor 9-mediated IFN-beta production in myeloid dendritic cells. Eur. J. Immunol. 37, 315–327.

Shaulian, E., and Karin, M. (2002). AP-1 as a regulator of cell life and death. Nat. Cell Biol. 4, E131–E136.

Singh, A., Singh, V., Tiwari, R.L., Chandra, T., Kumar, A., Dikshit, M., and Barthwal, M.K. (2016). The IRAK-ERK-p67phox-Nox-2 axis mediates TLR4, 2-induced ROS production for IL-1β transcription and processing in monocytes. Cell. Mol. Immunol. 13, 745–763.

Smolinska, M.J., Page, T.H., Urbaniak, A.M., Mutch, B.E., and Horwood, N.J. (2011). Hck tyrosine kinase regulates TLR4-induced TNF and IL-6 production via AP-1. J. Immunol. 187, 6043–6051.

Stein, B., Baldwin, A.S., Jr., Ballard, D.W., Greene, W.C., Angel, P., and Herrlich, P. (1993). Cross-coupling of the NF-kappa B p65 and Fos/Jun transcription factors produces potentiated biological function. EMBO J. 12, 3879–3891.

Stepanek, O., Draber, P., and Horejsi, V. (2014). Palmitoylated transmembrane adaptor proteins in leukocyte signaling. Cell. Signal. 26, 895–902.

Swanson, J.A. (2008). Shaping cups into phagosomes and macropinosomes. Nat. Rev. Mol. Cell Biol. 9, 639–649.

Thalhamer, T., McGrath, M.A., and Harnett, M.M. (2008). MAPKs and their relevance to arthritis and inflammation. Rheumatology (Oxford) 47, 409–414.

Turner, M.D., Nedjai, B., Hurst, T., and Pennington, D.J. (2014). Cytokines and chemokines: at the crossroads of cell signalling and inflammatory disease. Biochim. Biophys. Acta 1843, 2563–2582.

Wall, A.A., Condon, N.D., Luo, L., and Stow, J.L. (2019). Rab8a localisation and activation by Toll-like receptors on macrophage macropinosomes. Philos. Trans. R. Soc. Lond. B Biol. Sci. 374, 20180151.

Yoshida, S., Hoppe, A.D., Araki, N., and Swanson, J.A. (2009). Sequential signaling in plasma-membrane domains during macropinosome formation in macrophages. J. Cell Sci. 122, 3250–3261.

Zewinger, S., Reiser, J., Jankowski, V., Alansary, D., Hahm, E., Triem, S., Klug, M., Schunk, S.J., Schmit, D., Kramann, R., et al. (2020). Apolipoprotein C3 induces inflammation and organ damage by alternative inflammasome activation. Nat. Immunol. 21, 30–41.

STAR★METHODS

KEY RESOURCES TABLE

REAGENT or RESOURCE	SOURCE	IDENTIFIER
Antibodies		
phospho-c-Fos (Ser-32), clone D82C12	Cell Signaling Technology	Cat#5348; RRID: AB_10557109
phospho-C/EBPβ (Thr-235)	Cell Signaling Technology	Cat#3084; RRID: AB_2260359
phospho-NF-κB p65 (Ser-536), clone 93H1	Cell Signaling Technology	Cat#3033; RRID: AB_331284
phospho-c-Jun (Ser-63), clone E6I7P	Cell Signaling Technology	Cat#91952
c-Fos, clone 9F6	Cell Signaling Technology	Cat#2250; RRID: AB_2247211
NF-κB p65, clone D14E12	Cell Signaling Technology	Cat#8242; RRID: AB_10859369
GAPDH, clone 14C10	Cell Signaling Technology	Cat#2118; RRID: AB_561053
phospho-Akt (Ser-473), clone D9E	Cell Signaling Technology	Cat#4060; RRID: AB_2315049
Grb2	Cell Signaling Technology	Cat#3972; RRID: AB_10693935
Csk, clone C74C1	Cell Signaling Technology	Cat#4980; RRID: AB_2276592
SLP65/BLNK, clone D8R3G	Cell Signaling Technology	Cat#12168; RRID: AB_2756401
Lyn, clone C13F9	Cell Signaling Technology	Cat#2796; RRID: AB_2138391
phospho-Src Family (Tyr-416), clone D49G4	Cell Signaling Technology	Cat#6943; RRID: AB_10013641
Erk1/2, clone 137F5	Cell Signaling Technology	Cat#4695; RRID: AB_390779
phospho-Erk1/2, clone D13.14.4E	Cell Signaling Technology	Cat#4370; RRID: AB_2315112
Lamin A/C, clone 4C11	Cell Signaling Technology	Cat#4777; RRID: AB_10545756
β-tubulin, clone 9F3	Cell Signaling Technology	Cat#2128; RRID: AB_823664
TLR4, clone 76B357.1	Abcam	ab22048; RRID: AB_446735
Erk1/2, clone EPR17526	Abcam	ab184699; RRID: AB_2802136
V5 antibody, clone SV5-PK1	Bio-Rad/AbD Serotec	MCA1360; RRID: AB_322378
SCIMP	Luo et al., 2017	N/A
Alexa Fluor 488	Molecular Probes	A21206; RRID: AB_2535792
anti-Mouse IgG (H+L) HRP	Thermo Fisher Scientific	G-21040; RRID: AB_2536527
anti-Rabbit IgG (H+L) HRP	Thermo Fisher Scientific	G-21234; RRID: AB_2536530
Mouse IL-6, clone MP5-20F3	BD OptEIA	Cat#554400; RRID: AB_398549
Mouse IL-6 Biotin, clone MP5-32C11	BD OptEIA	Cat#554402; RRID: AB_395368
Mouse IL-12p40, clone C15.6	BD OptEIA	Cat#551219; RRID: AB_394097
Mouse IL-12p40 Biotin, clone C17.8	BD OptEIA	Cat#554476; RRID: AB_395419
Bacterial and virus strains		
E.Coli BL21-CodonPlus (DE3)-RP	Agilent Technologies	Cat#230255
Chemicals, peptides, and recombinant proteins		
4′,6-Diamidino-2′-phenylindole dihydrochloride (DAPI)	Sigma-Aldrich	Cat#32670
Rhodamine Phalloidin	Molecular Probes	R415
Alexa Fluor 647 Phalloidin	Molecular Probes	A22287
JF 549 HaloTag	L.Lavis (Janelia, Ashburn, VA)	N/A
LPS from Salmonella enterica serotype minnesota Re 595	Sigma-Aldrich	L9764
Human EGF Recombinant Protein	Thermo Fisher Scientific	PHG0311
U0126	Sigma-Aldrich	U120
Recombinant human M-CSF/CSF-1	ImmunoTools GmbH	Cat#11343118
Lipofectamine 2000	Thermo Fisher Scientific	Cat#11668019
488-Dextran 70,000 MW	Thermo Fisher Scientific	D7173
Critical commercial assays		
Mouse TNF ELISA kit	BD OptEIA	Cat#558534
Mouse IL-10 AlphaLISA kit	Perkin Elmer	AL502

(Continued on next page)

Continued

REAGENT or RESOURCE	SOURCE	IDENTIFIER
Experimental models: Cell lines		
Mal$^{-/-}$, Trif$^{-/-}$, Trif$^{-/-}$/Tram$^{-/-}$ iBMMs	Dr Ashley Mansell, Hudson Institute of Medical Research, Melbourne, Australia	N/A
RAW264.7	ATCC	TIB-71
CRISPR/Cas9-mediated SCIMP knockout (KO) RAW264.7	Luo et al., 2017	N/A
CRISPR/Cas9-mediated SCIMP knockout (KO) RAW264.7 stably expressing SCIMP-V5	Luo et al., 2017	N/A
Experimental models: Organisms/strains		
C57BL/6N-Scimp$^{tm1a(KOMP)Wtsi}$/Mmucd	Mutant Mouse Resource and Research Center	RRID: MMRRC_049566-UCD
C57BL6/J-Cbp$^{-/-}$	Animal Resources Centre, Murdoch, WA, Australia	N/A
C57BL/6J	In-house breeding colony	N/A
Oligonucleotides		
Primer: gblock_TSP-2XMyc: TGCTGACCCCGCCGTTGCTCCTGCTGCTGCCCCTGCTCTCAGCTCTGGTCGCGGCGGCTATCGACGCCGAGCAGAAACTCATCTCTGAAGAGGATCTGGCT	This paper	N/A
Primer: gblock_Halo_SCIMP_ PmeI _F: CCGGTCATCATCACCATCACTGAGTTTAAACCCGCTGATCAGCCTCGACTG	This paper	N/A
Primer: gblock_Halo_SCIMP_BamHI_R: ACCACACTGGACTAGTGGATCCGACGCGTTATCGCTCTGAAAGTACAG	This paper	N/A
Primer: Erk2- KpnI-F: AATTGGTACCGCCACCATGGCGGCGGCGGCG	This paper	N/A
Primer: Erk2-BamHI-R: AATTGGATCCCGAGATCTGTATCCTGGCTGGAATCTAGCAGTCTCT	This paper	N/A
siRNA: mScimp #1: sense sequence: 5′-AGACAACCCUCAGCUUGGUACUCAU-3′	Luo et al., 2017	N/A
siRNA: mScimp #1: antisense sequence: 5′-AUGAGUACCAAGCUGAGGGUUGUCU-3′	Luo et al., 2017	N/A
siRNA: control (mHdac1 #1): sense sequence: 5′-GAACUACCCACUGCGAGACGGCAUU-3′	Luo et al., 2017	N/A
siRNA: control (mHdac1 #1): antisense sequence: 5′-AAUGCCGUCUCGCAGUGGGUAGUUC-3′	Luo et al., 2017	N/A
See Table S1 for details of real time primers used in this study	This paper	N/A
Recombinant DNA		
pGEX-6P-1-GST-SCIMP-T1	Luo et al., 2017	N/A
pGEX-6P-1-GST-SCIMP-T1-Y58F	Luo et al., 2017	N/A
pGEX-6P-1-GST-SCIMP-T1-Y96F	Luo et al., 2017	N/A
pGEX-6P-1-GST-SCIMP-T1-Y120F	Luo et al., 2017	N/A
pGEX-6P-1-GST-SCIMP-T2	Luo et al., 2017	N/A
pGEX-6P-1-GST-TLR4-TIR	Luo et al., 2017	N/A
pEF6-TSP-Halo-SCIMP-V5	This paper	N/A
pEF6-GFP-Erk2	This paper	N/A
Software and algorithms		
ProteinPilot v6	AB Sciex	https://sciex.com/products/software/proteinpilot-software

(*Continued on next page*)

Continued

REAGENT or RESOURCE	SOURCE	IDENTIFIER
GraphPad Prism 9	GraphPad	http://www.graphpad.com/scientific-software/prism
Zeiss Zen 2	Zeiss	https://www.zeiss.com/microscopy/int/products/microscope-software/zen.html
Zeiss Zen Black	Zeiss	https://www.zeiss.com/microscopy/int/products/microscope-software/zen.html
SlideBook 6	3i	https://www.intelligent-imaging.com/slidebook
Image Lab	Bio-Rad	https://commerce.bio-rad.com/en-au/product/image-lab-software
ImageJ	Schindelin et al., 2012	https://imagej.net/software/fiji
arivis Vision4D 3.3	Arivis	https://imaging.arivis.com/en/imaging-science/arivis-vision4d

RESOURCE AVAILABILITY

Lead contact
Further information and requests for resources and reagents should be directed to and will be fulfilled by the Lead Contact, Lin Luo (l.luo@imb.uq.edu.au).

Materials availability
All unique reagents generated in this study are available from the Lead Contact with a completed Materials Transfer Agreement and reasonable compensation by the requestor for their processing and shipping.

Data and code availability
All data reported in this paper will be shared by the Lead Contact upon request.

This paper does not report original code. Any additional information required to reanalyze the data reported in this paper is available from the Lead Contact upon request.

EXPERIMENTAL MODEL AND SUBJECT DETAILS

Animals
Male and female mice of 8-12 weeks of age were used for this study. Mice were housed with rodent chow and water *ad libitum* in groups of up to five animals per cage in a specific pathogen-free (SPF) facility with a 12-hour light/dark cycle. For wild-type primary macrophages, C57BL/6J mice were obtained from an in-house breeding colony. $Scimp^{-/-}$ mice (strain C57BL/6N-Scimp$^{tm1a(KOMP)Wtsi}$/Mmucd, RRID: MMRRC_049566-UCD) were obtained from the Mutant Mouse Resource and Research Center (MMRRC) at University of California at Davis, an NIH-funded strain repository, and was donated to the MMRRC by The KOMP Repository, University of California, Davis; Originating from Ramiro Ramirez-Solis, CSD. $Scimp^{+/+}$ and $Scimp^{+/-}$ littermates were used as controls as indicated. $Pag/Cbp^{-/-}$ mice (C57BL6/J-Cbp$^{-/-}$) were obtained from the Animal Resources Centre (Murdoch, WA, Australia).

Cell lines
Bone marrow cells were collected from femurs and tibias of 8-12 week old mice and *ex vivo* differentiated in RPMI 1640 medium supplemented with 2 mM L-glutamine (Invitrogen, VIC, Australia), 10% heat-inactivated fetal bovine serum, 50 U/ml penicillin and 50 μg/ml streptomycin (Thermo Fisher Scientific, Australia) and 100 ng/ml purified recombinant macrophage colony stimulating factor–1 (CSF-1) (11343118; ImmunoTools GmbH) over 7 days at 37°C in humidified 5% CO_2 to obtain BMMs as previously described (Luo et al., 2017). Immortalized $Mal^{-/-}$, $Trif^{-/-}$ and $Trif^{-/-}/Tram^{-/-}$ BMMs (generously provided by Dr Ashley Mansell, Hudson Institute of Medical Research, Melbourne, Australia) were cultured in the same media as BMMs without the addition of CSF-1. RAW264.7 cells (ATCC) were maintained in RPMI 1640 medium supplemented with 2 mM L-glutamine (Invitrogen, VIC, Australia) and 10% heat-inactivated fetal bovine serum. Generation of CRISPR/Cas9-mediated SCIMP knockout (KO) RAW264.7 cells and reconstituted SCIMP-V5 stable cell line has previously been described (Luo et al., 2017). All cells were cultured at 37°C in humidified 5% CO_2.

Bacterial Strains
DNA constructs were transformed into chemically competent *E.Coli* BL21-CodonPlus (genotype: *E. coli* B F$^-$ ompT hsdS(r$_B^-$ m$_B^-$) dcm$^+$ Tet^r gal endA Hte [argU proL Cam^r]) and cultured in sterile LB Broth bacterial growth media at 37°C for 16 h with shaking.

Ethics statement
All studies involving animals and use of primary mouse cells were reviewed and approved by the appropriate animal ethics committee at University of Queensland (approval number: IMB/351/19).

METHOD DETAILS

Generation of DNA constructs and protein expression
GST-SCIMP T1 (amino acids 29–150) and GST-SCIMP-T2 (amino acids 93–150) were produced by PCR amplification from full-length mouse SCIMP cDNA and subcloned into the pGEX-6P-1 vector (Luo et al., 2017). GST-SCIMP-T1 (Y58F, Y96F and Y120F) were generated using a QuikChange site-directed mutagenesis kit (Stratagene). GST-TLR4-TIR (amino acids 670–835) was produced from pET28a-TIR4-TIR (Luo et al., 2017) and subcloned into pGEX6P-1. All constructs were confirmed by DNA sequencing at the Australian Genome Research Facility (AGRF, Brisbane, Australia). GST fusion proteins were expressed in *E. coli* and purified using glutathione-Sepharose beads (Amersham Biosciences). For design of Halo-tagged expressible SCIMP construct (pEF6-TSP-Halo-SCIMP-V5), a gBlocks gene fragment containing the transmembrane signal peptide (TSP) and 2xMyc-tag was designed and ordered from IDT Technologies (Singapore) (Key resources table). The gene fragment was inserted into an empty pEF6-V5-HIS-TOPO backbone (Catalog number: K961020, Thermo Fisher Scientific, Australia) via Gibson Assembly as per manufacturer's instruction (NEBiolabs, Australia). HaloTag was digested out of a pEF1α-Halo-Rab13 plasmid (Condon et al., 2018) using restriction digest (NheI and AsiSI) and the HaloTag fragment was ligated into the newly formed pEF6 backbone with the gBlocks gene fragment. BamHI and PmeI were inserted into pef6-TSP-Halo vector by using PCR and gblock_Halo_SCIMP primer sets (Key resources table). The SCIMP gene was digested out of the pEF6/V5-His TOPO TA-SCIMP construct (Luo et al., 2020) by using BamHI and PmeI restriction enzymes. The SCIMP fragment was then purified and inserted into the pEF6 backbone now containing the TSP, Myc-tag, BamHI/PmeI restriction sites and HaloTag via Gibson Assembly. The final construct as well as intermediate stages were sequenced for accuracy. The mouse Erk2 full-length construct was amplified by PCR from cDNA using two primers (Key resources table), and then cloned into the pEF6-GFP-N1 vector and confirmed by DNA sequencing.

siRNA-mediated gene silencing and DNA transfection
siRNA knockdown of SCIMP in BMMs was performed at day 6 using electroporation as previously described (Luo et al., 2017, 2020). Briefly, cells were resuspended in complete media at a concentration of 5×10^6 cells/350 μl with addition of 10 μl 1 M HEPES (tissue culture grade) per ml of cells. 350 μl of the cell suspension was transferred to 0.4 cm electroporation cuvettes and mixed with siRNAs against SCIMP or HDAC1 (control gene) to a final concentration of 0.5 μM or tissue culture grade water (no siRNA control) in a final volume of 400 μl. Cells were electroporated at 240 V, 1,000 μF and ∞ Ω and washed twice before plating at the appropriate cell number. Cells were treated with indicated stimuli at 24 h post-electroporation. siRNA sequences are listed in the Key resources table. Transient transfection of Halo-SCIMP and GFP-Erk2 into RAW264.7 cells was performed using Lipofectamine 2000 (Thermo Fisher Scientific, Australia) according to the manufacturer's instructions.

Immunoblotting
BMMs were lysed in radioimmunoprecipitation assay (RIPA) buffer (50 mM Tris–HCl, 150 mM NaCl, 1% Triton X-100, 0.5% sodium deoxycholate, 0.1% sodium dodecyl sulfate) with cOmplete Mini protease and PhosSTOP phosphatase inhibitors (Sigma-Aldrich Castle Hill, NSW, Australia). For nuclear and cytoplasmic fractionation, BMMs were lysed using an NE-PER Nuclear and Cytoplasmic Extraction Kit (78833, Thermo Fisher Scientific, Australia) following the manufacturer's instructions. Protein was quantified by bicinchoninic acid assay (Thermo Fisher Scientific, Australia) and boiled in sodium dodecyl sulfate polyacrylamide gel electrophoresis (SDS–PAGE) sample buffer for 5 min at 95°C. Following separation on 10% SDS-PAGE, proteins were transferred to a polyvinylidene difluoride membrane (Bio-strategy, Tingalpa QLD, Australia), blocked with 5% BSA (Sigma-Aldrich Castle Hill, NSW, Australia) or 5% skim milk in tris-buffered saline (TBS)/0.1% Tween-20 and incubated with primary antibodies diluted 1:1000 overnight at 4°C. After washing, membranes were incubated with secondary antibody diluted 1:10,000 for 1 h and chemiluminescence was developed using ECL detection reagent (Thermo Fisher Scientific, Australia) and imaged using a ChemiDoc and Image Lab Software (Bio-Rad Laboratories, Hercules, CA, USA). Densitometry analysis was performed using ImageJ Fiji version 2.1.0/1.53c (National Institutes of Health, MD, USA).

Affinity pull down and co-immunoprecipitation
RAW267.4 cells, iBMMs or BMMs from SCIMP mice were stimulated with 100 ng/ml LPS for 30 min as indicated and lysed in lysis buffer (20 mM Tris pH 7.4, 150 mM NaCl, 1% NP-40, 5% glycerol, cOmplete Mini protease and PhosSTOP phosphatase inhibitors (Sigma-Aldrich Castle Hill, NSW, Australia)). Lysates were incubated with GST, GST-SCIMP-T1/T2/Y58F/Y96F/Y120F and GST-TLR4-TIR Sepharose beads in MicroSpin columns (GE Healthcare) for 16 h at 4°C. Beads were washed with ice-cold wash buffer (20 mM Tris, 150 mM NaCl, 1% NP-40, pH 7.4) and bound protein was eluted by boiling in 2 × SDS-PAGE sample buffer for 5 min at 95°C. For immunoprecipitation experiments, control or 30 min LPS-treated RAW264.7 cells stably expressing SCIMP-V5 or *Scimp*^{+/+} or *Scimp*^{−/−} BMMs were lysed in lysis buffer as above and cleared lysates were incubated with anti-V5 or anti-Erk1/2 antibody-bound protein G agarose beads (Thermo Fisher Scientific, Australia) for 16 h at 4°C. Beads were washed with lysis buffer

and bound protein were eluted in 2x SDS-PAGE sample buffer. For pull down and immunoprecipitation experiments proteins were separated by 10% SDS-PAGE and analyzed by immunoblotting.

Mass spectrometry

LC MS/MS analysis of binding partners from a GST-SCIMP-T1 pull down in RAW263.7 cells was performed on a Shimadzu Prominence Nano HPLC (Japan) coupled to a Triple TOF 5600 mass spectrometer (ABSCIEX, Canada) equipped with a nano electrospray ion source (IMB Mass Spectrometry Facility, The University of Queensland) (Luo et al., 2014b, 2017). Peptide extracts (6 μl) were injected onto a 50 mm × 300 μm C18 trap column (Agilent Technologies, Australia) at 30 μl min^{-1} and desalted for 5 min using 0.1% formic acid at 30 μl min^{-1}. The trap column was then placed in-line with the analytical nano high-performance liquid chromatography column and a 150 mm × 75 μm 300SBC18 column (Agilent Technologies, Australia) for mass spectrometry analysis. Linear gradients of 1%–40% solvent B over 35 min at a flow rate of 300 nl min^{-1}, followed by a gradient from 40 to 80% solvent B in 5 min were used for peptide elution. Solvent B was held at 80% for 5 min for washing the column and returned to 1% solvent B for equilibration, before injection of the next sample. Solvent A consisted of 0.1% formic acid and solvent B contained 90/10 acetonitrile/0.1% formic acid. The ion spray voltage was set to 2,400 V, declustering potential (DP) 100 V, curtain gas flow 25, nebulizer gas 1 (GS1) 12 and interface heater at 150 °C. The mass spectrometer acquired 500 ms full-scan time-of-flight mass spectrometry (TOF-MS) data followed by 20 by 50 ms full-scan product ion data in an information-dependent acquisition mode. Full-scan TOF-MS data were acquired over the mass range 350–1,400 and for product ion ms/ms 80–1,400. Ions observed in the TOF-MS scan exceeding a threshold of 100 counts and a charge state of +2 to +5 were set to trigger the acquisition of product ion, ms/ms spectra of the resultant 20 most intense ions. The data were acquired and processed using Analyst TF 1.6.1 software (ABSCIEX, Canada). Proteins were identified by database searching using ProteinPilot v6 (ABSCIEX, Canada) against the UniProt_Sprot database. Search parameters were defined as a thorough search using trypsin digestion and all entries in the database. Proteins were considered identified if there was at least one peptide identified with 99% confidence (mass spectrometry score at least 2).

Gene expression and cytokine analysis

Total RNA was extracted from cells and DNaseI-treated using an RNeasy Mini Kit following the manufacturer's instructions (QIAGEN, VIC, Australia) and RNA concentrations were determined using a NanoDrop ND-1000 (Thermo Fisher Scientific, Australia). 1 μg RNA was reverse transcribed into cDNA using oligoDT primers and SuperScript III (Invitrogen, VIC, Australia). Gene expression was quantified using SYBR Green (Applied Biosystems, Massachusetts, USA) RT-qPCR on an Applied Biosystems ViiA7 Real Time PCR system (Life Technologies/Thermo Fisher Scientific, Australia) using gene-specific primers (Table S1), with expression determined using the ΔCt method and normalized to *Hprt*.

For quantification of cytokine secretion, BMMs (1x10^6 cells/ml) were treated with 100 ng/ml LPS for 8 h or 24 h and supernatants were collected and analyzed for levels of secreted cytokines using a BD OptEIA ELISA kit (mouse TNF 558534) or paired antibodies (IL-6 554400/554402 and IL-12p40 551219/554476) (BD Biosciences, Australia) or AlphaLISA kit (mouse IL-10, AL502, Perkin Elmer, VIC, Australia) following the manufacturer's instructions. Absorbance was measured at 450 nm (BD OptEIA) or with excitation and emission at 680 nm and 615 nm respectively (AlphaLISA) using a Tecan Infinite M1000 Pro microplate reader (Thermo Fisher Scientific, Australia) and analyzed using GraphPad Prism 9 (San Diego, CA, USA).

Immunofluorescence & fixed cell imaging

BMMs were grown on #1.5 coverslips and fixed in 4% paraformaldehyde (PFA) and permeabilized with 0.1% Triton X-100 for 5 min before immunolabelling with primary antibodies diluted 1:500 in 0.5% bovine serum albumin/PBS for 1 h at RT. After washing, cells were incubated in secondary antibody diluted 1:400 in 0.5% bovine serum albumin/PBS with Rhodamine Phalloidin (R415) and 4′,6-Diamidino-2′-phenylindole dihydrochloride (DAPI) for 1 h at RT. Coverslips were mounted on microscope slides using ProLong Diamond mountant (Thermo Fisher Scientific, Australia) and sealed with nail polish. 5 phase shift images were acquired on an Axio Imager M2 with Apotome.2 fitted with a Plan Neofluar 40x NA 1.3 oil objective and illuminated with a CoolLED light source and captured in Zeiss Zen 2 software with a Zeiss Axiocam 506 camera (Zeiss, Oberkochen, Germany).

For RAW264.7 cells transfected with Halo-SCIMP and GFP-Erk2, cells were grown on #1.5 coverslips and incubated with 10 nM JF 549 HaloTag ligand for 30 min at 37°C, washed with PBS and fixed in 4% paraformaldehyde (PFA) and permeabilized with 0.1% Triton X-100 before being incubated with phalloidin-647 diluted in 0.5% BSA/PBS for 45 min and mounted on microscope slides using ProLong Diamond mountant (Thermo Fisher Scientific, Australia) and sealed with nail polish. Cells were imaged with a Zeiss LSM 880 Confocal using Fast Airyscan mode on an Axiovert 200 Inverted Microscope with a Plan Apochromat 63x NA 1.4 oil objective and using Zeiss Zen Black software (Zeiss, Oberkochen, Germany).

Live cell imaging of dextran uptake

RAW264.7 cells stably expressing SCIMP-V5 were grown on 35 mm MatTek glass bottom dishes. Cells were incubated with 10 nM JF 549 HaloTag ligand for 30 min at 37°C before incubation with 488-Dextran (70,000 MW) (Thermo Fisher Scientific, Australia) and 100 ng/ml LPS for 30 min prior to imaging. Time series images were captured using a Zeiss LSM 880 Confocal on an Axiovert 200 Inverted Microscope with a Plan Apochromat 63x NA 1.4 oil objective and using Zeiss Zen Black software (Zeiss, Oberkochen, Germany).

Lattice light sheet live cell imaging

For LLSM, CRISPR/Cas9-mediated SCIMP KO RAW264.7 cells were transfected with Halo-SCIMP and GFP-Erk2 and plated at 0.2×10^6 cells/ml on 5 mm round #1 coverslips. Halo-549 ligand was added to the cells 30 min prior to imaging. For LLSM imaging, cells were incubated CO^2-free in L-15 medium (supplied with 10% FCS 2 mM L-glutamine and 10 mg/ml Pen/Strep) and stimulated with 100 ng/ml LPS (Sigma-Aldrich). Image volumes of at least 106x53x75 μm (XYZ) were imaged continuously for 20 min at 3.2 s intervals, consisting of at least 151 planes at 10 ms exposures/channel sequentially. Imaging was carried out using a 3i lattice light-sheet V2 microscope, samples were illuminated with a Coherent Sapphire 488 nm diode laser at and MPB Communications 560 nm diode laser both at 1%–2% AOTF transmittance through an excitation objective (Special Optics 28.6 × 0.7 NA 3.74-mm water dipping lens) at an angle of 31.8 degrees. Individual sheets were generated using 3i Slidebook software (488 nm 52 beams, 0.960 μm spacing, 560 nm 45 beams, 1.102 μm spacing both with a cropping factor of 0.150 μm and spacing factor of 0.970) through a 0.550/0.493 NA annular mask. Fluorescence signal was detected with a Nikon 25x 1.1 NA CFI Apo LWD objective and 2.5X tube lens (62.5x total system magnification) using 2x Hamamatsu Orca Flash 4.0 V2 sCMOS cameras running SlideBook 6 software (3i, Colorado, USA). Post processing of LLSM data includes GPU-accelerated deskewing and 10-40 cycles of deconvolution based on the Richard-Lucy algorithm (Microvolution, California, USA).

QUANTIFICATION AND STATISTICAL ANALYSIS

Image analysis

All image analysis was carried out in ImageJ (Fiji version 2.1.0/1.53c)(Schindelin et al., 2012). For nuclear translocation analysis in Figures 7C and S4B, c-Fos and NF-κB fluorescent signal intensity was measured in nuclear regions segmented from DAPI signal. For LLSM images in Figures 4B and 4C, co-localization between image channels was calculated from maximum and sum intensity projections using the AND function in image calculator and visualized using FireLUT. 4D renders in Video S4 were created using Arivis Vision4D 3.3 software.

Statistics

All datasets subjected to statistical analysis were compiled from at least 3 independent experiments as indicated. All data are presented as arithmetic mean ± SEM. Student's t test was used for direct comparison of a single experimental variable. For datasets containing multiple comparisons between three or more groups, a one-way or two-way analysis of variance (ANOVA) was performed with post-test as indicated. In all statistical analyses, a *P* value < 0.05 was considered statistically significant and descriptions of individual *P* values calculated for each experimental comparison are stated in the respective figure legends. Statistics were calculated using GraphPad Prism 9 (San Diego, CA, USA).